

Scientific paper

# Nickel Removing by Electrocoagulation of Ni(II)-NH<sub>3</sub>-CO<sub>2</sub>-SO<sub>2</sub>-H<sub>2</sub>O System. Kinetics, Isothermal, Mechanism and Estimated Cost of Operation

# Armando Rojas Vargas,<sup>1,\*</sup> Margarita Penedo Medina,<sup>2</sup> Alba González Vives,<sup>3</sup> Noureddine Barka<sup>4</sup> and Aymara Ricardo Riverón<sup>5</sup>

<sup>1</sup> Empresa de Servicios Técnicos de Computación, Comunicaciones y Electrónica "Rafael Fausto Orejón Forment", Nicaro, Holguín, Cuba

<sup>2</sup> Universidad de Oriente, Facultad de Ingeniería Química, Santiago de Cuba, Cuba

<sup>3</sup> POLYMAT, Departamento de Ciencia y Tecnología de Polímeros, Universidad del País Vasco, España

<sup>4</sup> Sultan Moulay Slimane University of Beni Mellal, Multidisciplinary Research and Innovation Laboratory, FP Khouribga, BP.145, 25000, Khouribga, Morocco.

<sup>5</sup> Centro de Investigaciones del Níquel "Alberto Fernández Montes de Oca", Nicaro, Holguín, Cuba

\* Corresponding author: E-mail: arojas@eros.moa.minem.cu) Tel: +53-24-51-6695

Received: 02-09-2022

#### Abstract

This study reports nickel removing by electrocoagulation of Ni(II)-NH<sub>3</sub>-CO<sub>2</sub>-SO<sub>2</sub>-H<sub>2</sub>O system at laboratory scale. Experiments were done using Al/Al pair electrodes at initial nickel concentration between 293 and 1356 mg L<sup>-1</sup> and under operation parameters of pH 8.6, current density 9.8 mA cm<sup>-2</sup>, electrolysis time 30 min, and temperature 60 °C. The obtained results show removal efficiencies between 97.7 and 99.7%. Kinetics modeling suggested combined effects of external diffusion and nucleation, and as controlling step the chemical reaction and a possible autocatalytic contribution. The process followed the Langmuir's isotherm with a maximum adsorption capacity of 7519 mg g<sup>-1</sup>. ICP-OES, XRD and FTIR characterization of the precipitates indicated a typical Ni-Al layered double hydroxide structures with 33.4–40.7% nickel and 6.3–7.0% aluminum depending on initial nickel concentration. The operation costs of energy and electrode consumption were 320–537 \$ t<sup>-1</sup> of removed nickel.

Keywords: Electrocoagulation - isotherm - kinetic - layered double hydroxides -mechanism - nickel removing

# 1. Introduction

In the production plant located in Punta-Gorda Cuba, the Ammoniacal Carbonate Leaching Technology is used for the selective recovering of nickel and cobalt form lateritic ore. In the distillation effluents a suspension of basic nickel carbonate is obtained. After sedimentation of this suspension, the clear liquor contained several ionic species with composition according to the following proportions: 1.8 < Ni/S < 3.2, 1.5 < NH<sub>3</sub>/CO<sub>2</sub> < 2.0, 10.4 < CO<sub>2</sub>/S < 13.8 of the Ni(II)-NH<sub>3</sub>-CO<sub>2</sub>-SO<sub>2</sub>-H<sub>2</sub>O system. The temperature of the liquor is between 70 and 85 °C and the pH from 7.4 to 9.0.2

The dissolved nickel in the clear liquor reaches concentrations between 0.2 and 1.0 g  $\rm L^{-1}$  in the form of hydroxide and coordination compounds. It precipitates with NH<sub>4</sub>HS in a piston flow reactor leading to nickel sulfide. The reagents used in this process are toxic, corrosive and of high hazard for the environment. For these reasons, the possibility of substituting chemical precipitation by electrocoagulation (EC) process was analyzed in our previous study.  $^4$ 

The EC consists of the destabilization of suspended, emulsified or dissolved compounds in an electrolytic cell facilitating their removal.<sup>5</sup> In relation to the mechanisms of the process, the fundamental stages have been reported:<sup>6–12</sup>

- 1 Electrolytic reactions on the surface of the electrodes.
- 2 Formation of coagulants in the aqueous phase.
- 3 Destabilization and adsorption of pollutants on coagulants (coagulation).
- 4 Aggregation of destabilized particles and formation of flocs (flocculation).
- 5 Removal of contaminating material by means of secondary treatment.

It also refers to the contribution of mechanisms functioning synergistically and benefit the removal efficiency such as: chemistry precipitation by the formation of the pollutant metal hydroxides, reduction of metal ions, non-metal inions and gases formation at the cathode surface, co-precipitation and complexation of anions and organic compounds.<sup>8,9,11,13</sup>,

The parameters that influence the efficiency of the EC process can be classified into two categories: design parameters and operational parameters. The most important design parameters are related with material, shape, arrangement and spacing of electrodes, as well as type of power supply; either direct current (DC), alternating current (AC) or alternating pulsed current (APC). The operational parameters are current density, electrocoagulation time, aqueous solution pH, temperature, agitation speed, initial ions concentration and supporting electrolyte. 4,7,8,10,13,14,15

The most favorable conditions for the nickel removal from Ni(II)-NH<sub>3</sub>-CO<sub>2</sub>-SO<sub>2</sub>-H<sub>2</sub>O system by EC using Al/Al pair electrodes were determined through a full-factorial experimental design.<sup>4</sup> The optimum efficiency of 95% was achieved for a current density of 9.8 mA cm<sup>-2</sup>, temperature of 60 °C, solution pH of 8.65 and 660 mg L<sup>-1</sup> of initial nickel concentration. This resulted in a specific energy consumption of 5.41 kWh per kg of Ni.

Many authors have identified the formation of Hydrotalcite-like layered double hydroxides (LDHs) during EC process. Zhao (2010) proposed the formation of Mg/Al-F-LDH as one of the mechanisms for EC defluoridation in systems containing both F<sup>-</sup> and Mg<sup>2+</sup>.<sup>16</sup> Mendoza, et al. (2018) in-situ synthesized Mg/Al-LDH using synthetic water under laboratory-scale conditions, with aluminum and AZ31 magnesium alloys electrodes at 5 mA cm<sup>-2</sup>, the coagulants were generated through electrochemical oxidation of the electrodes.<sup>17</sup> Jiang (2021) in-situ synthetized Zn/Al-LDH for the removal of strontium in a simulated liquid radioactive waste.<sup>18</sup> Finally, Ou (2021) fabricated Ni/Fe-LDH using nickel-plating wastewater.<sup>19</sup>

LDHs are represented by the general formula  $[M^{2+}_{1-x}M^{3+}_{x}(OH)_{2}]^{x+}(A^{n-}_{x/n})$  mH<sub>2</sub>O, where  $M^{2+}$  is a divalent cation  $(Mg^{2+}, Ca^{2+}, Mn^{2+}, Co^{2+}, Ni^{2+}, Cu^{2+}, Zn^{2+})$ ,  $M^{3+}$ , is a trivalent cation  $(Al^{3+}, Cr^{3+}, Mn^{3+}, Fe^{3+}, Co^{3+}, Ni^{3+})$ ,  $A^{n-}$ , interlayer anion  $(Cl^{-}, NO_{3}^{-}, ClO_{4}^{-}, CO_{3}^{2-}, SO_{4}^{2-}, S_{2}O_{3}^{2-}$  and other organic compounds), and x is the charge density for the molar ratio  $M^{3+}(M^{2+} + M^{3+})^{-1}$  which varied from 0.2 and 0.35. $^{20-31}$  These compounds have been extensively investigated due to their improved

microstructure, increased active electrochemical sites and their wide applications.

In the case of Ni/Al-LDH, it has been reported as highly efficient in the adsorption of metals (Au, Cd, Cu, Pb, Se), 28,32 anions (F-,  $IO_3^-$ )<sup>33,34</sup> and organic compounds. <sup>24–26,29,35,36</sup> Ni-based LDHs in the energy storage and conversion field are still limited by their intrinsically poor conductivity, aggregation, limited active sites and stability.<sup>23,31</sup> Ni/Al-LDH exhibits a specific capacitance 2128 F g<sup>-1</sup> at 1 A g<sup>-1</sup> and coulombic efficiency above 80% during 1000 cycles (Ni/ Al:3).<sup>37,38</sup> In order to improve the electrochemical performance, nanostructured Ni/Al-LDH have been synthetized using different routes. <sup>23,39,40,41</sup> This compound, followed by controlled thermal decomposition, represents an appropriate material for the preparation of ceramic pigments with different properties.<sup>42</sup> Carbonate intercalated with a c-axis preferred orientation, show excellent anticorrosive performance with polarization current density of 10<sup>-9</sup> A cm<sup>-2</sup>.<sup>43</sup> It is active for the photocatalytic conversion of CO2 to CO in water, under UV light irradiation,44 and promising catalyst precursors for fine CO2 removal from hydrogen-rich gas streams through the methanation reaction and methane dry reforming. 45,46 Moreover, the combination of nickel and aluminum finds applications in the production of superalloys (53.3  $\leq$  Ni  $\leq$  73.0%, 1.2  $\leq$  Al  $\leq$  6.0%) and permanent magnets  $(15 \le Ni \le 26\%, 8 \le Al \le 12\%)$ .

It was assumed that the thermodynamics, kinetics, equilibrium analysis through adsorption isotherms, characterization of the adsorbent, and the analysis of chemical-physical interactions through Stern's electrical double layer model, coordination surface and the electrode processes, provide elements to propose the removal mechanism by electrocoagulation. 30,47,48

The purpose of this work was to determine the reaction kinetics, the adsorption isotherm, the mechanism and the preliminary cost of operation for the nickel removing by electrocoagulation from the Ni(II)-NH<sub>3</sub>-CO<sub>2</sub>-SO<sub>2</sub>-H<sub>2</sub>O system, at different concentrations of dissolved nickel in the initial liquor. The resulted precipitate was characterized by ICP-OES, DXR, and FTIR in order to elucidate the removal mechanics.

# 2. Materials and Methods

#### 2. 1. Materials

The liquor used in the electrocoagulation experiments was sampled spot in the distillation columns discharge at the production plant in Punta-Gorda Cuba. The pH was adjusted with ammonium carbonate solution (pH 11.7) or a mixture of hydrochloric and nitric acid. The initial nickel concentration was adjusted by dilution of the liquor using distilled water. The resulting concentrations for each sample are shown in Table 1. The material used as electrode was aluminum with a composition of 98.98% Al, 0.5% Mg, 0.33% Fe and 0.114% Si.

 $\label{lem:table 1.} \textbf{Characterization of the liquor fed to the electrocoagulation cell}$ 

Ni (mg L <sup>-1</sup> )	$ NH_3 $ $ (g L^{-1}) $	$CO_2 \ (g L^{-1})$	S (g L <sup>-1</sup> )	$[SO_4]^{2-}$ $(g L^{-1})$	
293	0.51	0.33	2.70	3.59	
379	0.92	0.50	2.14	3.52	
474	1.10	0.25	2.43	3.53	
505	1.08	0.29	2.31	3.46	
646	1.40	0.30	2.73	5.70	
775	1.20	0.35	3.00	3.46	
953	1.21	0.35	3.47	6.83	
1356	4.70	3.27	3.20	6.82	

#### 2. 2. Methods

EC experiments were done in an electrochemical cell consisted of a discontinuous cylindrical glass reactor, with a useful capacity of 500 mL. It was equipped with a pair of flat electrodes, arranged vertically, in parallel, 10 mm spacing, submerged 57 mm in the liquor with a total area of  $5.6\ 10^{-3}\ m^2$  and an effective area of  $4.6\ 10^{-3}\ m^2$ . The cell was alimented by Direct current source of  $0.01\ -30$  V, maximum amperage 10 A, power supply  $220\ \pm10\%$ , 50 Hz and 250 W. The current density was monitored using a multimeter. The positive terminal of the current source was connected directly to the electrode (anode) and the negative terminal to the multimeter and from this (COM) to the cathode. The source allowed to regulate the voltage to keep the electric current amperage constant (Fig.1).

nickel removal from the Ni(II)-NH $_3$ -CO $_2$ -SO $_2$ -H $_2$ O system.  $^4$ 

The nickel removal, electrode mass and electric power consumption were determined at different concentration of nickel [Ni] dissolved in the initial liquor.

After each experiment, samples were removed from the reactor to a volumetric flask. Then, they were covered and allowed to settle for 24 h. Finally, the aliquot required for chemical analysis was pipetted. Residual nickel concentration was measured by atomic absorption spectroscopy (AAS) using a SP-9 Spectrophotometer.

The preparation of the electrodes consisted of polishing the surface with coarse and fine sandpaper, and washing with distilled water. After electrocoagulation, they were cleaned with phosphoric acid solution, sodium hexametaphosphate and distilled water until the deposited layer was removed. Later these electrodes were weighed. Each anode was used for at most two experiments. an Optical emission spectrometer GS 1000-II was used to characterize the electrodes.

The resulting precipitate was characterized using Inductively Coupled Plasma Optical Emission Spectrometry (ICP-OES), Spectro ARCOS FHX. X-ray diffraction (XRD), Bruker D8 Advance equipment, Cu anode lamp (CuK $\alpha$  radiation) and wavelength 1.5405 Å, constant scanning at a measurement interval of 2theta (2 $\theta$ ) between 5 – 6 to 100° with a step of 0.05° measured every 5 min, and Fourier transform infrared spectroscopy (FTIR), Nicolet 6700 Spectrometer, range between 4000 and 400 cm<sup>-1</sup>, resolution of 4 cm<sup>-1</sup>.

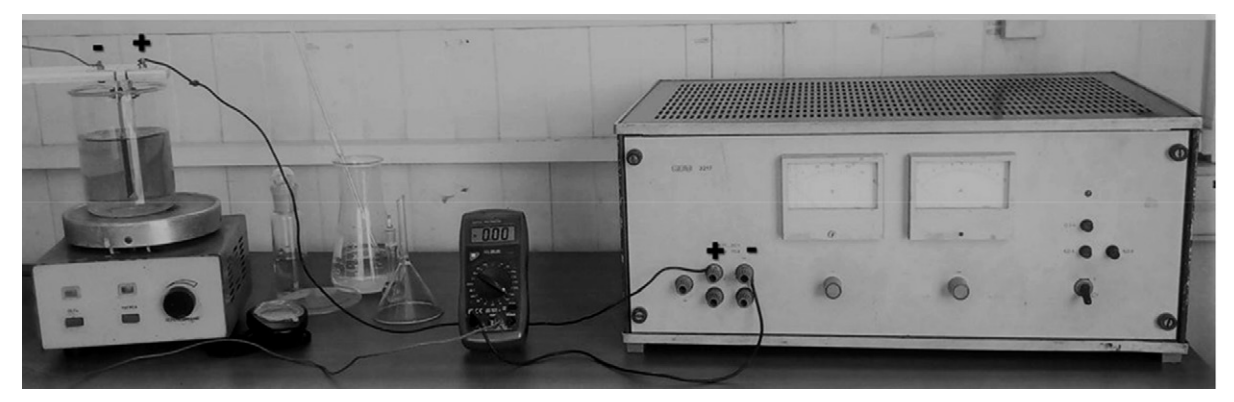


Figure 1. Experimental installation of electrocoagulation

The overflow liquor from the basic nickel carbonate settler tank was first adjusted to the desired pH using a Philips PW-9420 pH meter and the temperature was controlled ASCON KR3 controller. The it was fed to the reactor and continually stirred at 100 rpm using a hot plate stirrer with thermal control.

The nickel removal experiments by electrocoagulation consisted in assuming the current density of 9.8 mA cm<sup>-2</sup>, pH 8.6, temperature 60 °C and electrolysis time 30 min, according to the most favorable conditions for the

#### 2. 3. Adsorption Kinetics Models

The adsorption capacity  $(Q_t)$  or amount of adsorbate adsorbed per adsorbent unit  $(mg\ g^{-1})$  was determined by Eq. (1).

$$Q_t = (C_0 - C_t) \cdot \frac{V}{\Delta M_F} \tag{1}$$

where  $C_0$  (mg  $L^{-1}$ ) is the initial concentration of nickel,  $C_t$  (mg  $L^{-1}$ ) is the concentration of nickel in the liquid phase in each time interval, V (L) is the volume of solution,  $\Delta MF$ 

(g) is the amount of metal in solution according to Faraday's Law, Eq. (2).

$$\Delta M_F = \frac{I \cdot M \cdot t}{n \cdot F} \tag{2}$$

where, I (A) is the current intensity, M the molecular weight of [Al] 26.98 g mol<sup>-1</sup>, t (s) the electrocoagulation time, n number of electrons for aluminum (3), F Faraday constant (96487 c mol<sup>-1</sup>).

When the duration of the process is long enough,  $Q_t$  is constant and determines the charge or adsorption capacity ( $Q_e$ , mg  $L^{-1}$ ) corresponding to the concentration at equilibrium ( $C_e$ , mg  $L^{-1}$ ).

Kinetics data were correlated to pseudo-second order, Avrami, Elovich, Bangham and Weber-Morris intra-particle diffusion models.  $^{48,49,50}$  The parameters were adjusted with StatGraphic 5.1 and Microsoft Excel and the best quality of fit was decided by the highest coefficient of determination ( $\mathbb{R}^2$ ).

The pseudo-second order kinetic model is presented by Eq. (3) and its linear form is given by Eq. (4):

$$\frac{dQ_t}{dt} = k_2 \cdot (Q_e - Q_t)^2 \tag{3}$$

$$\frac{t}{Q_t} = \frac{1}{k_2 \cdot Q_e^2} + \frac{1}{Q_e} \cdot t = \frac{1}{h} + \frac{1}{Q_e} \cdot t \tag{4}$$

where  $k_2$  (g mg<sup>-1</sup> min<sup>-1</sup>) is the adsorption rate constant while h (g<sup>-1</sup> mg min<sup>-1</sup>) is assumed as the initial reaction rate.

Avrami's fractional kinetic model is based on the Johnson-Mehl-Avrami-Erofeev-Kolmogorov (JMAEK) theory,<sup>51</sup> and consist of phase transformations via homogenous and spontaneous nucleation and growth of a crystal as a function of crystallization time. Although it has been assumed as an empirical model for the analysis of adsorption kinetic data.<sup>47</sup> It is represented by Eq. (5), integrated form (6) and linearized form (7).

$$\frac{dQ_t}{dt} = k_{av}^{n_{av}} \cdot t^{n_{av}-1} \cdot (Q_e - Q_t) \tag{5}$$

$$Q_t = Q_e \cdot \{1 - exp[-(k_{av} \cdot t)^{n_{av}}]\}$$
 (6)

$$ln\left[-\ln\left(1-\frac{Q_t}{Q_e}\right)\right] = n_{av} \cdot \ln k_{av} + n_{av} \cdot \ln t \tag{7}$$

where,  $k_{av}$  (min<sup>-1</sup>) is the kinetic constant or global constant,  $n_{av}$  (/) fractional reaction order, which refers to the nucleation, growth and orientation of crystallites or possible changes in the adsorption mechanism.

The Elovich kinetic model in its nonlinear and linear form is expressed by the Eq. (8) and (9), respectively.

$$\frac{dQ_t}{dt} = \alpha \cdot exp(\beta \cdot Q_t) \tag{8}$$

$$Q_t = \frac{1}{\beta} \cdot \ln(\alpha \cdot \beta) + \frac{1}{\beta} \cdot \ln(t)$$
 (9)

where,  $\alpha$  (mg g<sup>-1</sup> min<sup>-1</sup>) is a constant related to adsorption rate,  $\beta$  (g mg<sup>-1</sup>) is a constant which depicts the extent of surface coverage.

Bangham's equation was used to evaluate whether the adsorption is pore-diffusion controlled, it is represented by Eq. (10).

$$lnln\left(\frac{c_0}{c_0 - Q_t \cdot W}\right) = ln\left(k_B \cdot W \cdot \frac{1}{V}\right) + \alpha \cdot ln t \quad (10)$$

where,  $C_0$  (mg·L<sup>-1</sup>) is initial concentration, V (mL) volume of the solution, W (g L<sup>-1</sup>) weight of the adsorbent,  $k_B$  (mL g<sup>-1</sup> L) and  $\alpha$ (/) the constants.

The Weber and Morris intraparticle diffusion model can be expressed by Eq. (11) and its linear form by Eq. (12).

$$\frac{\mathrm{dQ}_t}{\mathrm{d}t} = \frac{1}{2} \cdot k_3 \cdot t^{-1/2} \tag{11}$$

$$Q_t = k_3 \cdot \sqrt{t} + c \tag{12}$$

where,  $k_3$  (mg g<sup>-1</sup> min<sup>-0.5</sup>) the intra-particle diffusion rate constant, c (mg g<sup>-1</sup>) is the intercept.

In addition, the goodness of fit of several integral equations for the reaction kinetics was evaluated, in order to investigate the controlling mechanism in the nickel removing by electrocoagulation, regarding the individual or simultaneous contribution of the resistances: external diffusion, internal diffusion, nucleation, chemical reaction, autocatalysis (Table 2). 52,53,54 The algorithm followed consisted of assuming a controlling mechanism, calculating the fraction of incomplete conversion and adjusting the model with StatGraphic 5.1 and Microsoft Excel, the best quality of fit was decided by the highest coefficient of determination (R<sup>2</sup>) and the lowest estimated error, Eq. (13).

$$I = 1 - x = 1 - \left(\frac{C_0 - C_t}{C_0}\right) \tag{13}$$

where, I (/) fraction of incomplete conversion and x fractional conversion (/).

#### 2. 4. Adsorption Isotherm Models

The Langmuir, Freundlich, Temkin, Toth, Koble – Carrigan and Redlich – Peterson adsorption isotherm models were evaluated. 10,25,35,48,49,50

Langmuir's isotherm in the linear form is shown in Eq. (29), and the equilibrium parameter is defined in Eq. (30).

$$\frac{C_e}{Q_e} = \frac{C_e}{q_m} + \frac{1}{q_m \cdot K_L} \tag{29}$$

$$R_L = \frac{1}{1 + K_L \cdot C_0} \tag{30}$$

where,  $q_m$  (mg  $g^{-1}$ ) is the maximum monolayer adsorption capacity,  $K_L$  (L mg<sup>-1</sup>) the Langmuir adsorption constant that defines the affinity of the adsorbate for the adsorbent,

**Table 2.** Models used in the kinetic analysis to investigate the controlling mechanism in the nickel removing by electrocoagulation

Name	g(I, x)	Eq.			
	External diffusion				
1-D	1-I	(14)			
2-D	$1 - I^{\frac{1}{2}}$	(15)			
3-D	$1 - I^{\frac{1}{3}}$	(16)			
Boundary layer	$1 - I^{\frac{2}{3}}$	(17)			
	Internal diffusion				
1-D	$x^2$	(18)			
2-D	$I \cdot Ln(I) + x$	(19)			
3-D (Jander)	$\left(1-I^{\frac{1}{3}}\right)^2$	(20)			
3-D (Ginstling – Brounshtein) $1 - \frac{2}{3} \cdot x - I^{\frac{2}{3}}$					
	Nucleation				
Avrami	$[-ln(I)]^{\frac{1}{2}}$	(22)			
Erofeév	$[-ln(I)]^{\frac{1}{3}}$	(23)			
Avrami – Erofeév	$ln \cdot \left[ ln \left( rac{1}{I}  ight)  ight]$	(24)			
JMAEK	$5\cdot [-ln(I)]^{\frac{1}{5}}$	(25)			
	Autocatalysis				
Roginskii-Shultz	$\frac{2}{3} \cdot \frac{2}{3}$	(26)			
Kolmogorov	$\frac{2}{x^3} \cdot \frac{4}{1^3}$	(27)			
	Chemical reaction				
Power law	$1 - I^{\frac{1}{3}}$	(28)			

and  $R_L$  is the equilibrium parameter of the Langmuir's isotherm.

Freundlich's isotherm is applicable to adsorption processes that occur on heterogonous surfaces, its linear form is expressed by Eq. (31).

$$lnQ_e = \frac{1}{n} \cdot \ln C_e + \ln K_f \tag{31}$$

where,  $K_f$  (mg g<sup>-1</sup>)/(mg L<sup>-1</sup>)<sup>n</sup> is related to the adsorption capacity and n (dimensionless) is related to the adsorption intensity; it also indicates the relative distribution of the energy and the heterogeneity of the adsorbate sites.

Temkin isotherm model takes into account the effects of indirect adsorbate/adsorbate interactions on the adsorption process, Eq. (32) and (33).

$$Q_e = B \cdot \ln C_e + B \cdot \ln K_T \tag{32}$$

$$b_T = \frac{R \cdot T}{R} \tag{33}$$

where,  $b_T$  (J mol<sup>-1</sup>) is Temkin constant which is related to the heat of sorption and  $K_T$  (L mg<sup>-1</sup>) is Temkin isotherm constant, T (K) the absolute temperature, R is the gas constant 8.31 J mol<sup>-1</sup> K<sup>-1</sup>.

The Toth's isotherm is an empirical modification of the Langmuir equation, Eq. (34) and (35).

$$\frac{Q_e}{q_m} = \theta = \frac{K_e \cdot C_e}{[1 + (K_h \cdot C_e)^n]^{1/n}}$$
(34)

$$ln\frac{Q_e^n}{q_m^n - Q_e^n} = n \cdot ln(K_h) + n \cdot ln(C_e)$$
(35)

where,  $K_h$  (mg  $g^{-1}$ ) is Toth isotherm constant and n (mg  $g^{-1}$ ) is the Toth constant.

Koble-Carrigan isotherm model is a three-parameter equation which incorporates both Langmuir and Freundlich isotherms for representing equilibrium adsorption data, Eq. (36).

$$\frac{1}{Qe} = \left(\frac{1}{A_k \cdot C_e^n}\right) + \frac{B_k}{A_k} \tag{36}$$

where,  $A_k$  ( $L^n$   $mg^{1-n}$   $g^{-1}$ ),  $B_k$ , (L mg) $^n$ , n (dimensionless) are Koble - Carrigan's isotherm constants.

The Redlich-Peterson isotherm is a mix of the Langmuir and Freundlich isotherms. Its linear form can be expressed by the Eq. (37).

$$ln\left(\frac{C_e}{Q_e}\right) = \beta \cdot ln(C_e) - ln K_R \tag{37}$$

where,  $K_R$  (L  $g^{-1}$ ) is Redlich-Peterson isotherm constant,  $\beta$ (dimensionless) is constant.

The verification of the consistency of adsorption models and the theoretical assumptions of adsorption models was made by Average Relative Error (ARE) and Marquardt's Percent Standard Deviation (MPSD) calculated by Eq. (38) and (39) respectively.<sup>35</sup>

$$ARE = \frac{100}{n} \cdot \sum_{i=1}^{n} \left[ \left( \frac{Q_{e,i,cal} - Q_{e,i,exp}}{Q_{e,i,exp}} \right) \right]$$
(38)

$$MPSD = \sqrt{\frac{1}{n-P} \cdot \sum_{i=1}^{n} \left[ \left( \frac{Q_{e,i,cal} - Q_{e,i,exp}}{Q_{e,i,exp}} \right) \right]^{2}}$$
 (39)

where, n is the number of data points and P the number of parameters.

#### 2. 5. Operating Cost Estimate

The operating cost per kg of nickel removed was calculated by Eq. (40).

$$C_{op} = \left[ a \cdot C_{en} + b \cdot \Delta M_{exp} \right] \cdot \frac{1}{m_{Ni}} \tag{40}$$

where, Cop (\$ kg<sup>-1</sup>) operating cost, a (\$ 0.090 / kWh) cost

of electricity,  $C_{en}$  (kWh) power consumption, b (1.445 \$ kg<sup>-1</sup>) cost of the aluminum electrode;  $\Delta$ Mexp (g) experimental weight loss of the electrodes,  $m_{Ni}$  (kg) mass of nickel removed.

After transforming, the operating cost can be expressed as Eq. (41):

$$C_{op} = \left[ a \cdot U \cdot I \cdot t \cdot \frac{1}{60} + b \cdot \Delta M_{exp} \right] \cdot \frac{1}{[Ni] \cdot V \cdot x_{Ni}} \quad (41)$$

where, U (V) voltage, I (A) current intensity, t (min) electrocoagulation time, [Ni] (g  $L^{-1}$ ) initial concentration of dissolved nickel, V (0.5 L) useful volume of the cell,  $x_{Ni}$  fraction converted or nickel removing.

The current efficiency ( $\eta$ ) and the specific energy consumption per kg electrode dissolved (SEC, kW-h kg<sup>-1</sup>) were determined by Eq. (42) and (43), respectively.

$$\eta = \frac{\Delta M_{exp}}{\Delta M_E} \tag{42}$$

$$SEC = \frac{n \cdot F \cdot U}{3600 \cdot M \cdot \eta} \tag{43}$$

# 3. Results and Discussion

#### 3. 1 Adsorption Kinetics

The study of adsorption kinetics provides information on the mechanisms involved in the process. For the experimental conditions of 9.8 mA cm<sup>-2</sup>, 60 °C, pH 8.6, 30 min of electrolysis and initial concentration  $293 \le [Ni] \le 953$  mg L<sup>-1</sup>, the nickel removal efficiency was between  $99.0 \le X \le 99.7\%$  (Table 3).

Table 3. Efficiency of nickel removal by electrocoagulation

Ni (mg L <sup>-1</sup> )	293	379	474	505	646	775	953	1356 <sup>1</sup>
X (%)								

<sup>140</sup> min of electrolysis

A model was obtained that relates the conversion time (t) as a function of the fractional conversion (x), nickel initial concentration (mg L<sup>-1</sup>), mass of aluminum [Al] and the coefficients o constants a, b, c, d, e, f, Eq. (44).

$$t = \begin{cases} a \cdot \left[1 - (1 - x)^{\frac{1}{2}}\right] \\ +b \cdot \left[5 \cdot \left[-\ln(1 - x)\right]^{\frac{1}{5}}\right] \\ +c \cdot \left[1 - (1 - x)^{\frac{1}{3}}\right] \\ +d \cdot \left[x^{\frac{2}{3}} \cdot (1 - x)^{\frac{2}{3}}\right] \end{cases} \cdot [Ni]^{e} \cdot [Al_{t}]^{f}$$
(44)

From Faraday's law to determine the mass of dissolved aluminum, Eq. (45) is obtained.

$$t^{n} = \begin{cases} a \cdot \left[1 - (1 - x)^{\frac{1}{2}}\right] \\ +b \cdot \left[5 \cdot \left[-\ln(1 - x)\right]^{\frac{1}{5}}\right] \\ +c \cdot \left[1 - (1 - x)^{\frac{1}{3}}\right] \\ +d \cdot \left[x^{\frac{2}{3}} \cdot (1 - x)^{\frac{2}{3}}\right] \end{cases}$$
 (45)

where, the constant (n) refers to the conversion time, the resistance coefficient to external diffusion (a), nucleation (b), chemical reaction (c) and its autocatalytic contribution (d), the nickel exponent (e), and the coefficient  $(k_{Al})$  for the estimate of dissolved aluminum by Faraday's Law.

The parameters of the conversion time (CVT) model (45) are shown in Table 4 for the concentration ranges: 293  $\leq$  Ni  $\leq$  646 mg  $L^{-1};\,775 \leq$  Ni  $\leq$  1356 mg  $L^{-1};\,293 \leq$  Ni  $\leq$  1356 mg  $L^{-1}.$  It reflects between 99.18 and 99.88% of the variability in nickel removal. The coefficient of determination (R²) adjusted by the degrees of freedom (g.l.) allows compare this model with others with the same number of independent variables.

CVT model expresses that the nickel removing is determined by the combined effect of the resistances of the mechanisms:

- External diffusion (a), in the film or boundary layer to the adsorbent surface, by the two-dimensional (2-D) diffusion model.
- Nucleation and crystallization (b), by the JMAEK equation, which refers to the random formation and growth of the adsorption surface due to the hydrolysis and polymerization reactions of aluminum, giving rise to the species monomeric, polymeric, oligomeric aluminum and Al(OH)<sub>3</sub>, where the contaminants adsorption occurs (Ni<sup>2+</sup>, S<sub>x</sub>O<sub>y</sub><sup>z-</sup>, CO<sub>3</sub><sup>2-</sup>, NH<sub>3</sub>) in the active centers by electrostatic interaction and coordination surface, and subsequent crystallization; in competition with that nucleation that occurs when the deposits grow on the electrodes.

Table 4. CVT model constants by Eq. (45) and quality of fit

	n	а	b	с	d	e	$k_{Al} \cdot 10^{-1}$	2 R <sup>2</sup>	R <sup>2</sup> (g. l.)
1	0.2938	8.8582	1.1429	12.4190	10.4680	0.3054	1.4834	99.41	99.18
2	0.3029	0.9418	1.7497	16.7428	18.7548	0.2812	1.5661	99.91	99.88
3	0.2985	9.9782	2.6673	13.2262	20.1508	0.2337	1.5250	99.35	99.24

 $<sup>^{1}[\</sup>rm{Ni}]$  between 293 and 646 mg L  $^{-1};\,^{2}[\rm{Ni}]$  775 - 1356 mg L  $^{-1};\,^{3}[\rm{Ni}]$  293 - 1356 mg L  $^{-1}.$ 

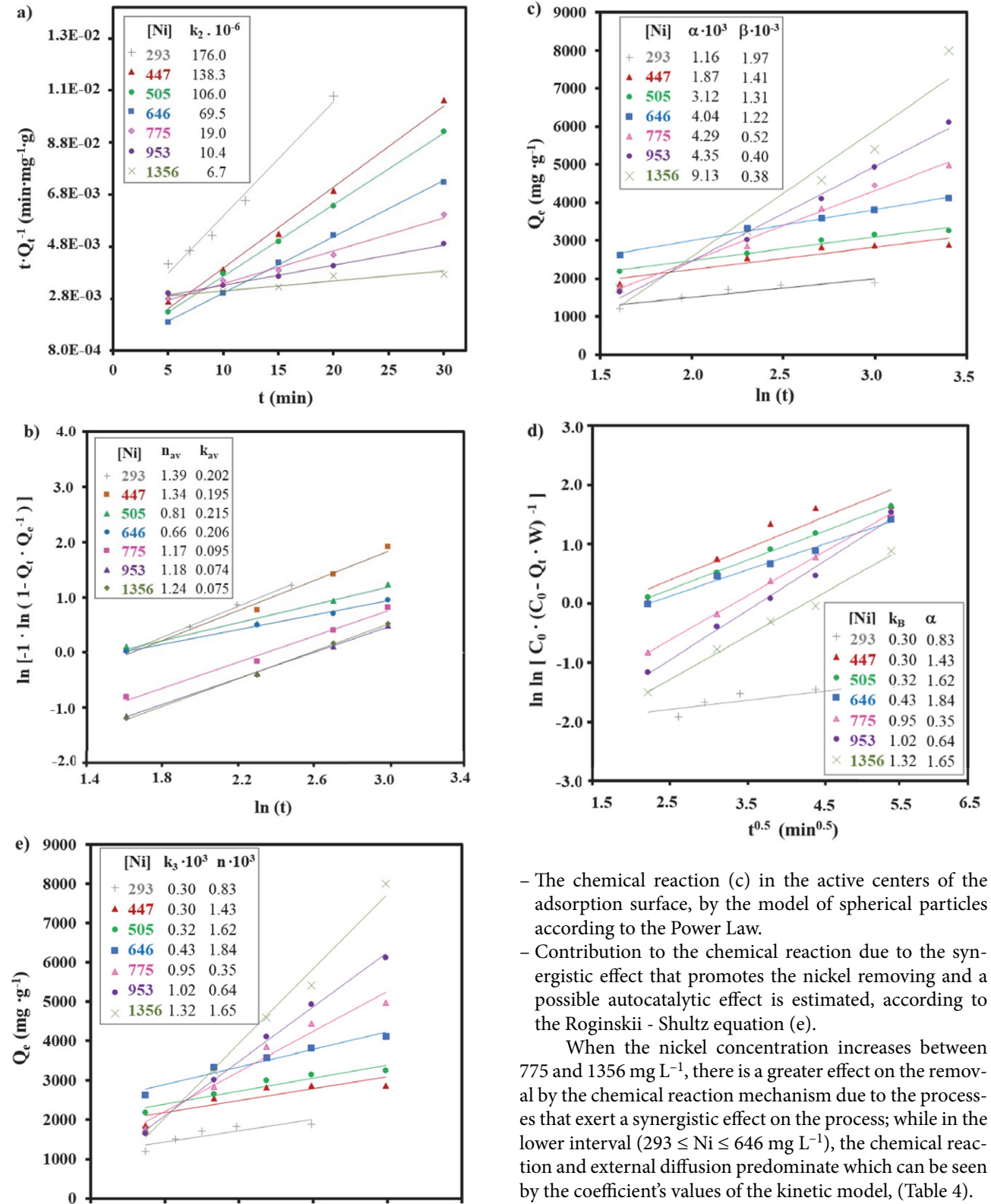


Figure 2. Adsorption of nickel with the electrode pair Al/Al at 9.8 mA cm<sup>-2</sup>, 60 °C, pH 8.6, a) Pseudo-second order kinetic model, b) Avrami's model, c) Elovich's model, d) Bangham's model, e) Weber and Morris's model.

3.5

4.5

 $t^{0.5}$  (min<sup>0.5</sup>)

5.5

2.5

1.5

When the nickel concentration increases between 775 and 1356 mg  $L^{-1}$ , there is a greater effect on the removal by the chemical reaction mechanism due to the processes that exert a synergistic effect on the process; while in the lower interval (293  $\leq$  Ni  $\leq$  646 mg L<sup>-1</sup>), the chemical reac-

2.5

3.0

[Ni]  $k_B$ 0.30

293

447

505 0.32 1.62

775 0.95 0.35

953 1.02 0.64

4.5

1356 1.32

3.5

0.83

1.65

6.5

0.30 1.43

0.43 1.84

5.5

tion and external diffusion predominate which can be seen by the coefficient's values of the kinetic model, (Table 4). The adsorption kinetic models were ordered by their

quality of fit: (1) pseudo 2nd order  $\approx$  (2) Avrami > (3) Elovich ≈ (4) Bangham >> (5) Weber-Morris. These were used to validate the conversion time model, Eq. (45).

The pseudo-second order (PSO) model showed a high quality of fit (96.1  $\leq$  R<sup>2</sup>  $\leq$  99.8%). As the initial nickel

6.5

concentration increased, (Fig.2 a), the rate constant  $k_2$  (g mg<sup>-1</sup> min<sup>-1</sup>) decreased. This result can be attributed to the progressive saturation of the active sites in the adsorption surface with the cation [Ni<sup>2+</sup>] and causes an increase in the necessary electrocoagulation time.

The Avrami´s model was representative of dates because of its high quality of fit. The removal rate  $(k_{av})$  for initial nickel concentration between 293 and 646 mg  $L^{-1}$  was assumed constant and equal to 0.20 (+/- 0.01) min $^{-1}$  (97.94  $\leq R^2 \leq$  99.62%); but in the range of 775 to 1356 mg  $L^{-1}$  the kinetic behavior changed and  $k_{av}$  decreased between 50 and 60% (98.82  $\leq$   $R^2 \leq$  99.75%) due to the increase in adsorbate concentration. It was regarded that in the first interval the contribution of the mechanism of external diffusion resistance influenced in the higher value of  $k_{av}$  while in the second interval  $k_{av}$  was lower under the mechanism control the chemical reaction resistance (Fig.2 b) (Table 4).

With respect to the lines slopes that reflect the fractional order  $(n_{av})$  of Avrami's model, in the interval  $293 \le [Ni^{2+}] \le 646$  mg  $L^{-1}$  decreased from 1.39 to 0.66 with the increase of the cation  $[Ni^{2+}]$ . This is attributed to the progressive saturation of the active adsorption sites because there is a greater amount of adsorbate that reaches the adsorbent surface and therefore a longer electrocoagulation time is required. Also, the interactions augment and the tendency to change the controlling mechanism. In the interval of  $775 \le [Ni^{2+}] \le 1356$  mg  $L^{-1}$ , the exponential constant  $(n_{av})$  increased to 1.21 (+/- 0.05). According to Eq. (44), it may be associated with the controlling mechanism of chemical reaction resistance.

The Elovich's model (95.5  $\leq$  R<sup>2</sup>  $\leq$  99.62%) suggests that the adsorbent active sites are heterogeneous and therefore exhibit different activation energies. This suggests that more than one mechanism incises the removal process such as transport in the solution phase (bulk diffusion) and surface diffusion. 48,49,50 The initial rate kinetic constant ( $\alpha$ ) (mg g<sup>-1</sup> min) increased proportionally to the concentration of [Ni<sup>2+</sup>]. In addition, the constant ( $\beta$ ) (g mg<sup>-1</sup>) related to the chemisorption activation energy and the extension of the adsorption surface, decreased with the increase of cation [Ni<sup>2+</sup>] throughout the interval (Fig.2 c).

The Bangham and Weber-Morris's models were less representatives of the data due to their lower quality of fit, in correspondence with the CVT model, Eq. (45) where internal diffusion resistance could be omitted from the process due to low statistical significance. The Bangham's model is applied to investigate pore activation for adsorbate diffusion. The fit quality was obtained in the interval  $95.0 \le R^2 \le 99.3\%$ , which indicates that both intra-particle diffusion and pore diffusion are not controlling in the process (Fig.2 d).<sup>50</sup> With regard to the Weber and Morris's model, it reflects the influence of external mass transfer followed by intra-particle diffusion in pores of different sizes.<sup>48,50</sup> The plot of  $Q_t$  versus  $t^{0.5}$  did not result in a linear relationship with intercept at the origin of coordinates  $(86.5 \le R^2 \le 99.1)$  (Fig.2 e). This result suggests that diffu-

sion is not a limiting step in the mechanism. Furthermore, the intra-particle kinetic rate constant was not directly proportional to the adsorbate concentration, suggesting that the process is not controlled by adsorption in the pores.

#### 3. 2 Nickel Adsorption Isotherms

The equilibrium concentration (Ce, mg  $L^{-1}$ ) corresponding to each initial nickel concentration ( $C_0$ , mg  $L^{-1}$ ), and the equilibrium adsorption capacity (Qe, mg  $g^{-1}$ ) were determined. From Fig.3 it can be seen that by increasing the initial concentration, the adsorption capacity at equilibrium increased. For  $[Ni^{2+}]>953$  mg  $L^{-1}$ , the formation of a plateau was obtained, which indicates saturation of the adsorption sites and a decrease in the removal efficiency at the experimental conditions studied.

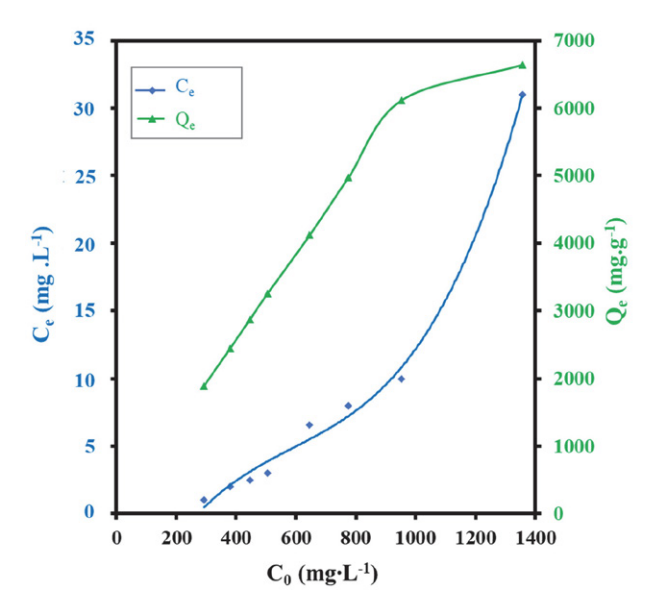


**Figure 3.** Equilibrium concentration ( $C_e$ ) and adsorption capacity ( $Q_e$ ) versus the initial concentration ( $C_0$ ) for nickel removing at 9.8 mA cm<sup>-2</sup>, 60 °C and pH 8.6.

Table 5 shows the isotherm constants for the adsorption of Ni(II) caclutated for rach isotherm model. That table indicates that the order of goodness-of-fit ( $\mathbb{R}^2$ ) of the adsorption isotherm models was: Langmuir (99.3%) > Redlich - Peterson (97.3%) > Koble - Carrigan (96.1%)  $\approx$  ToTh (96.1%) > Temkin (93.8%)  $\approx$  Freundlich (93.7%).

The Langmuir isotherm was more representative of the data, this presented the highest quality of fit determined by the coefficient of determination (R<sup>2</sup>), the lower ARE 7.6 and MPSD 0.013. This result suggests monolayer adsorption in a specific number and fixed of accessible sites on the adsorbent surface, all active sites have the same energy. Once an adsorbate occupies a site, no farther adsorption can occur on that site and there is not interaction

between adsorbate species. <sup>48,49,50</sup> The maximum adsorption capacity ( $q_m$ ) was 7519 mg g<sup>-1</sup>, the constant ( $K_L$ ) was 0.216 L mg<sup>-1</sup> and the equilibrium parameter 0.003  $\leq R_L \leq$  0.013.

The Redlich-Peterson's isotherm ( $K_{R~4.84~10}^{-4}~L~g^{-1}$ ; beta- $\beta$  0.61) and the Koble-Carrigan's isotherm ( $A_k$  1429  $L^n$  mg<sup>1-n</sup> g<sup>-1</sup>,  $B_k$  0.14 (L mg)<sup>n</sup>, n 1.08) refers that adsorption is a mixture (Langmuir and Freundlich) and not precisely the ideal adsorption monolayer. While the Toth's isotherm ( $K_h$  0.251 mg g<sup>-1</sup>, n 5.5 mg g<sup>-1</sup>) is a modification of the Langmuir's equation and suggest a heterogeneous adsorption (n > 1).

**Table 5.** Isotherm constants for the adsorption of Ni(II)

$\begin{array}{c ccccccccccccccccccccccccccccccccccc$	Parameter	Value									
$\begin{array}{c} K_L(L \ mg^{-1}) & 0.216 \\ R^2 & 99.30 \\ ARE & 7.60 \\ MPSD & 0.013 \\ \hline \hline \hline & Redlich - Paterson \\ K_R \ (L \ g^{-1}) & 4.84 \ 10^{-4} \\ (/) & 0.61 \\ R^2 \ (/) & 97.30 \\ ARE & 8.50 \\ MPSD & 0.017 \\ \hline \hline & Koble - Carrigan \\ A_k \ (L^n \ mg^{1-n} \ g^{-1}) & 1429 \\ B_k \ (L \ mg)^n & 0.14 \\ n \ (/) & 1.08 \\ R^2 \ (/) & 96.10 \\ ARE & 8.52 \\ MPSD & 0.026 \\ \hline \hline & Toth \\ q_m \ (mg \ g^{-1}) & 6650 \\ K_h \ (mg \ g^{-1}) & 0.251 \\ n \ (mg \ g^{-1}) & 5.50 \\ R^2 \ (/) & 96.10 \\ ARE & 10.00 \\ MPSD & 0.081 \\ \hline \hline & Temkin \\ K_T \ (L \ mg^{-1}) & 2.88 \\ b_T \ (J \ mol^{-1}) & 1.79 \\ R^2 \ (/) & 93.80 \\ ARE & 8.30 \\ MPSD & 0.015 \\ \hline \hline & Freundlich \\ n \ (/) & 2.51 \\ K_f \ (mg \ g^{-1})/(mg \ L^{-1})^n & 2001 \\ R^2 \ (/) & 93.70 \\ ARE & 8.31 \\ \hline \end{array}$	Langmu	ıir									
$\begin{array}{c} K_L(L \ mg^{-1}) & 0.216 \\ R^2 & 99.30 \\ ARE & 7.60 \\ MPSD & 0.013 \\ \hline \hline \hline & Redlich - Paterson \\ K_R \ (L \ g^{-1}) & 4.84 \ 10^{-4} \\ (/) & 0.61 \\ R^2 \ (/) & 97.30 \\ ARE & 8.50 \\ MPSD & 0.017 \\ \hline \hline & Koble - Carrigan \\ A_k \ (L^n \ mg^{1-n} \ g^{-1}) & 1429 \\ B_k \ (L \ mg)^n & 0.14 \\ n \ (/) & 1.08 \\ R^2 \ (/) & 96.10 \\ ARE & 8.52 \\ MPSD & 0.026 \\ \hline \hline & Toth \\ q_m \ (mg \ g^{-1}) & 6650 \\ K_h \ (mg \ g^{-1}) & 0.251 \\ n \ (mg \ g^{-1}) & 5.50 \\ R^2 \ (/) & 96.10 \\ ARE & 10.00 \\ MPSD & 0.081 \\ \hline \hline & Temkin \\ K_T \ (L \ mg^{-1}) & 2.88 \\ b_T \ (J \ mol^{-1}) & 1.79 \\ R^2 \ (/) & 93.80 \\ ARE & 8.30 \\ MPSD & 0.015 \\ \hline \hline & Freundlich \\ n \ (/) & 2.51 \\ K_f \ (mg \ g^{-1})/(mg \ L^{-1})^n & 2001 \\ R^2 \ (/) & 93.70 \\ ARE & 8.31 \\ \hline \end{array}$	$q_{\rm m}  ({\rm mg}  {\rm g}^{-1})$	7519									
$\begin{array}{c} R^2 & 99.30 \\ ARE & 7.60 \\ MPSD & 0.013 \\ \hline \hline & Redlich - Paterson \\ K_R (L g^{-1}) & 4.84  10^{-4} \\ (/) & 0.61 \\ R^2 (/) & 97.30 \\ ARE & 8.50 \\ MPSD & 0.017 \\ \hline \hline & Koble - Carrigan \\ A_k (L^n mg^{1-n} g^{-1}) & 1429 \\ B_k (L mg)^n & 0.14 \\ n (/) & 1.08 \\ R^2 (/) & 96.10 \\ ARE & 8.52 \\ MPSD & 0.026 \\ \hline \hline & Toth \\ q_m (mg g^{-1}) & 6650 \\ K_h (mg g^{-1}) & 0.251 \\ n (mg g^{-1}) & 5.50 \\ R^2 (/) & 96.10 \\ ARE & 10.00 \\ MPSD & 0.081 \\ \hline \hline & Temkin \\ K_T (L mg^{-1}) & 2.88 \\ b_T (J mol^{-1}) & 1.79 \\ R^2 (/) & 93.80 \\ ARE & 8.30 \\ MPSD & 0.015 \\ \hline \hline & Freundlich \\ n (/) & 2.51 \\ K_f (mg g^{-1})/(mg L^{-1})^n & 2001 \\ R^2 (/) & 93.70 \\ ARE & 8.31 \\ \hline \end{array}$	$K_L(L mg^{-1})$	0.216									
$\begin{array}{c ccccccccccccccccccccccccccccccccccc$		99.30									
$\begin{array}{c ccccccccccccccccccccccccccccccccccc$	ARE	7.60									
$\begin{array}{c} K_R  (L  g^{-1}) & 4.84  10^{-4} \\ (/) & 0.61 \\ R^2  (/) & 97.30 \\ ARE & 8.50 \\ MPSD & 0.017 \\ \hline \hline Koble - Carrigan \\ A_k  (L^n  mg^{1-n}  g^{-1}) & 1429 \\ B_k  (L  mg)^n & 0.14 \\ n  (/) & 1.08 \\ R^2  (/) & 96.10 \\ ARE & 8.52 \\ MPSD & 0.026 \\ \hline \hline Toth \\ q_m  (mg  g^{-1}) & 6650 \\ K_h  (mg  g^{-1}) & 0.251 \\ n  (mg  g^{-1}) & 5.50 \\ R^2  (/) & 96.10 \\ ARE & 10.00 \\ MPSD & 0.081 \\ \hline \hline Temkin \\ K_T  (L  mg^{-1}) & 2.88 \\ b_T  (J  mol^{-1}) & 1.79 \\ R^2  (/) & 93.80 \\ ARE & 8.30 \\ MPSD & 0.015 \\ \hline \hline Freundlich \\ n  (/) & 2.51 \\ K_f  (mg  g^{-1})/(mg  L^{-1})^n & 2001 \\ R^2  (/) & 93.70 \\ ARE & 8.31 \\ \end{array}$	MPSD	0.013									
$(/) \qquad \qquad 0.61 \\ R^2 \ (/) \qquad \qquad 97.30 \\ ARE \qquad \qquad 8.50 \\ MPSD \qquad \qquad 0.017 \\ \hline \hline \begin{array}{c} \textbf{Koble - Carrigan} \\ A_k \ (L^n \ mg^{1-n} \ g^{-1}) \qquad 1429 \\ B_k \ (L \ mg)^n \qquad \qquad 0.14 \\ n \ (/) \qquad \qquad 1.08 \\ R^2 \ (/) \qquad \qquad 96.10 \\ ARE \qquad \qquad 8.52 \\ MPSD \qquad \qquad 0.026 \\ \hline \hline \begin{array}{c} \textbf{Toth} \\ \\ Q_m \ (mg \ g^{-1}) \qquad \qquad 6650 \\ K_h \ (mg \ g^{-1}) \qquad \qquad 0.251 \\ n \ (mg \ g^{-1}) \qquad \qquad 5.50 \\ R^2 \ (/) \qquad \qquad 96.10 \\ ARE \qquad \qquad 10.00 \\ MPSD \qquad \qquad 0.081 \\ \hline \hline \begin{array}{c} \textbf{Temkin} \\ \\ K_T \ (L \ mg^{-1}) \qquad \qquad 2.88 \\ b_T \ (J \ mol^{-1}) \qquad \qquad 1.79 \\ R^2 \ (/) \qquad \qquad 93.80 \\ ARE \qquad \qquad 8.30 \\ MPSD \qquad \qquad 0.015 \\ \hline \hline \begin{array}{c} \textbf{Freundlich} \\ n \ (/) \qquad \qquad 2.51 \\ K_f \ (mg \ g^{-1})/(mg \ L^{-1})^n \qquad \qquad 2001 \\ R^2 \ (/) \qquad \qquad 93.70 \\ ARE \qquad \qquad 8.31 \\ \hline \end{array}$	Redlich - Paterson										
$\begin{array}{c} R^2  (/) & 97.30 \\ ARE & 8.50 \\ \hline MPSD & 0.017 \\ \hline \hline & \textbf{Koble - Carrigan} \\ A_k  (L^n  \text{mg}^{1-n}  \text{g}^{-1}) & 1429 \\ B_k  (L  \text{mg})^n & 0.14 \\ n  (/) & 1.08 \\ R^2  (/) & 96.10 \\ \hline & \textbf{ARE} & 8.52 \\ \hline MPSD & 0.026 \\ \hline \hline & \textbf{Toth} \\ q_m  (\text{mg}  \text{g}^{-1}) & 6650 \\ K_h  (\text{mg}  \text{g}^{-1}) & 0.251 \\ n  (\text{mg}  \text{g}^{-1}) & 5.50 \\ R^2  (/) & 96.10 \\ \hline & \textbf{ARE} & 10.00 \\ \hline & \textbf{MPSD} & 0.081 \\ \hline \hline & \textbf{Temkin} \\ \hline & \textbf{K}_T  (L  \text{mg}^{-1}) & 2.88 \\ b_T  (J  \text{mol}^{-1}) & 1.79 \\ R^2  (/) & 93.80 \\ \hline & \textbf{ARE} & 8.30 \\ \hline & \textbf{MPSD} & 0.015 \\ \hline \hline & \textbf{Freundlich} \\ n  (/) & 2.51 \\ K_f  (\text{mg}  \text{g}^{-1}) / (\text{mg}  \text{L}^{-1})^n & 2001 \\ R^2  (/) & 93.70 \\ \hline & \textbf{ARE} & 8.31 \\ \hline \end{array}$	$K_R (L g^{-1})$	$4.84 \ 10^{-4}$									
$ \begin{array}{c ccccccccccccccccccccccccccccccccccc$		0.61									
$\begin{array}{c ccccc} & \textbf{Koble - Carrigan} \\ & A_k  (L^n  mg^{1-n}  g^{-1}) & 1429 \\ B_k  (L  mg)^n & 0.14 \\ n  (/) & 1.08 \\ R^2  (/) & 96.10 \\ ARE & 8.52 \\ MPSD & 0.026 \\ \hline & & & & & & & & \\ \hline & & & & & & \\ \hline & & & &$	$R^{2}(/)$	97.30									
$ \begin{array}{c ccccccccccccccccccccccccccccccccccc$	ARE	8.50									
$\begin{array}{cccccccccccccccccccccccccccccccccccc$	MPSD	0.017									
$\begin{array}{cccccccccccccccccccccccccccccccccccc$		rigan									
$\begin{array}{c} n \ (/) & 1.08 \\ R^2 \ (/) & 96.10 \\ ARE & 8.52 \\ \hline MPSD & 0.026 \\ \hline \hline \hline & & & & \\ \hline Toth & & & \\ q_m \ (mg \ g^{-1}) & 6650 \\ K_h \ (mg \ g^{-1}) & 0.251 \\ n \ (mg \ g^{-1}) & 5.50 \\ R^2 \ (/) & 96.10 \\ ARE & 10.00 \\ \hline MPSD & 0.081 \\ \hline \hline & & & \\ \hline Temkin & & & \\ K_T \ (L \ mg^{-1}) & 2.88 \\ b_T \ (J \ mol^{-1}) & 1.79 \\ R^2 \ (/) & 93.80 \\ ARE & 8.30 \\ MPSD & 0.015 \\ \hline \hline & & & \\ \hline Freundlich & & \\ n \ (/) & 2.51 \\ K_f \ (mg \ g^{-1})/(mg \ L^{-1})^n & 2001 \\ R^2 \ (/) & 93.70 \\ ARE & 8.31 \\ \hline \end{array}$		1429									
$\begin{array}{cccccccccccccccccccccccccccccccccccc$		0.14									
$\begin{array}{c ccccccccccccccccccccccccccccccccccc$		1.08									
$\begin{array}{c c} \textbf{MPSD} & 0.026 \\ \hline & \textbf{Toth} \\ \textbf{Q}_m  (\text{mg g}^{-1}) & 6650 \\ \textbf{K}_h  (\text{mg g}^{-1}) & 0.251 \\ \textbf{n}  (\text{mg g}^{-1}) & 5.50 \\ \textbf{R}^2  (/) & 96.10 \\ \textbf{ARE} & 10.00 \\ \textbf{MPSD} & 0.081 \\ \hline & \textbf{Temkin} \\ \textbf{K}_T  (\textbf{L}  \text{mg}^{-1}) & 2.88 \\ \textbf{b}_T  (\textbf{J}  \text{mol}^{-1}) & 1.79 \\ \textbf{R}^2  (/) & 93.80 \\ \textbf{ARE} & 8.30 \\ \textbf{MPSD} & 0.015 \\ \hline & \textbf{Freundlich} \\ \textbf{n}  (/) & 2.51 \\ \textbf{K}_f  (\text{mg g}^{-1})/(\text{mg L}^{-1})^n & 2001 \\ \textbf{R}^2  (/) & 93.70 \\ \textbf{ARE} & 8.31 \\ \hline \end{array}$	$R^2$ (/)	96.10									
$\begin{array}{c ccccccccccccccccccccccccccccccccccc$		8.52									
$\begin{array}{cccccccccccccccccccccccccccccccccccc$	MPSD	0.026									
$\begin{array}{c} K_h  (mg  g^{-1}) & 0.251 \\ n  (mg  g^{-1}) & 5.50 \\ R^2  (\prime) & 96.10 \\ ARE & 10.00 \\ \hline MPSD & 0.081 \\ \hline \hline {\color{red} {\bf Temkin}} \\ K_T  (L  mg^{-1}) & 2.88 \\ b_T  (J  mol^{-1}) & 1.79 \\ R^2  (\prime) & 93.80 \\ ARE & 8.30 \\ MPSD & 0.015 \\ \hline {\color{red} {\bf Freundlich}} \\ n  (\prime) & 2.51 \\ K_f  (mg  g^{-1})/(mg  L^{-1})^n & 2001 \\ R^2  (\prime) & 93.70 \\ ARE & 8.31 \\ \hline \end{array}$											
$\begin{array}{cccc} n \ (mg \ g^{-1}) & 5.50 \\ R^2 \ (\prime) & 96.10 \\ ARE & 10.00 \\ MPSD & 0.081 \\ \hline \hline & & & \\ \hline & & & $	$q_{\rm m}  ({\rm mg  g^{-1}})$	6650									
$\begin{array}{cccccccccccccccccccccccccccccccccccc$		0.251									
$\begin{array}{c ccccc} ARE & 10.00 \\ MPSD & 0.081 \\ \hline & & & \\ \hline & & \\ \hline & & & \\ \hline & & \\ $		5.50									
$\begin{array}{c c} \text{MPSD} & 0.081 \\ \hline & \textbf{Temkin} \\ K_T \ (\text{L mg}^{-1}) & 2.88 \\ b_T \ (\text{J mol}^{-1}) & 1.79 \\ R^2 \ (\prime) & 93.80 \\ \text{ARE} & 8.30 \\ \text{MPSD} & 0.015 \\ \hline & \textbf{Freundlich} \\ n \ (\prime) & 2.51 \\ K_f \ (\text{mg g}^{-1})/(\text{mg L}^{-1})^n & 2001 \\ R^2 \ (\prime) & 93.70 \\ \text{ARE} & 8.31 \\ \hline \end{array}$	$R^2$ (/)	96.10									
$\begin{array}{c ccccccccccccccccccccccccccccccccccc$	ARE	10.00									
$\begin{array}{cccc} K_T  (L  mg^{-1}) & 2.88 \\ b_T  (J  mol^{-1}) & 1.79 \\ R^2  (/) & 93.80 \\ ARE & 8.30 \\ \hline MPSD & 0.015 \\ \hline \hline & & & & \\ \hline Freundlich & & & \\ n  (/) & & 2.51 \\ K_f  (mg  g^{-1})/(mg  L^{-1})^n & 2001 \\ R^2  (/) & 93.70 \\ ARE & 8.31 \\ \end{array}$	MPSD	0.081									
$\begin{array}{cccc} b_T \ (J \ mol^{-1}) & 1.79 \\ R^2 \ (/) & 93.80 \\ ARE & 8.30 \\ \hline MPSD & 0.015 \\ \hline \hline & & \\ \hline Freundlich & & \\ n \ (/) & & 2.51 \\ K_f \ (mg \ g^{-1})/(mg \ L^{-1})^n & 2001 \\ R^2 \ (/) & 93.70 \\ ARE & 8.31 \\ \hline \end{array}$		n									
$\begin{array}{ccc} R^2  (/) & 93.80 \\ ARE & 8.30 \\ MPSD & 0.015 \\ \hline & & \\ \hline Freundlich & \\ n  (/) & 2.51 \\ K_f  (mg  g^{-1})/(mg  L^{-1})^n & 2001 \\ R^2  (/) & 93.70 \\ ARE & 8.31 \\ \end{array}$		2.88									
$\begin{tabular}{lll} ARE & 8.30 \\ \hline MPSD & 0.015 \\ \hline \hline & & \\ \hline \hline & & \\ \hline \hline & & \\ \hline &$		1.79									
$\begin{tabular}{lll} MPSD & 0.015 \\ \hline \hline & Freundlich \\ n~(/) & 2.51 \\ K_f~(mg~g^{-1})/(mg~L^{-1})^n & 2001 \\ R^2~(/) & 93.70 \\ ARE & 8.31 \\ \hline \end{tabular}$											
$\begin{tabular}{cccccccccccccccccccccccccccccccccccc$											
$\begin{array}{lll} n \ (\ ) & 2.51 \\ K_f \ (mg \ g^{-1}) / (mg \ L^{-1})^n & 2001 \\ R^2 \ (\ ) & 93.70 \\ ARE & 8.31 \end{array}$	MPSD	0.015									
$\begin{array}{lll} K_f(mgg^{-1})/(mgL^{-1})^n & 2001 \\ R^2(/) & 93.70 \\ ARE & 8.31 \end{array}$											
R <sup>2</sup> (/) 93.70 ARE 8.31											
ARE 8.31	$K_f (mg g^{-1})/(mg L^{-1})^n$										
	* *										
MPSD 0.015											
	MPSD	0.015									

The Temkin's model assumes linear rather than logarithm decrease of heat of adsorption while ignoring extremely low and very high concentration. It also assumes uniform distribution of bounding energy up to some maximum bonding energy.<sup>35,50</sup> The heat of adsorption,  $b_T$  is equal to 1.79 J mol<sup>-1</sup> and  $K_T$  was 2.88 L mg<sup>-1</sup>.

Eventually, the lower value of the determination coefficient corresponded to the Freundlich's isotherm, which assumes a heterogeneous distribution of active sites and energy on the surface, applicable to multilayer adsorption.  $^{48,50}$  K<sub>f</sub> was 2001 (mg g<sup>-1</sup>)/(mg L<sup>-1</sup>)<sup>n</sup> and n was 2.51.

Thus, the kinetic and equilibrium analyses suggest the control of chemisorption on a monolayer, at a fixed and specific number of accessible sites on the adsorbent surface. Although, it does not specifically follow the ideal adsorption monolayer at identical sites. The interaction between the molecules is not neglected, due to the action of electrostatic forces and exchange reactions in the active sites of the coordination surface. In addition, the transport of solute through the internal structure of the adsorbent pores and the diffusion in the solid are neglected.

# 3. 3 Analysis of the Precipitate

In order to investigate the nickel removal mechanism by electrocoagulation the precipitate was analyzed. The ICP-OES, DXR and FTIR analysis showed the formation of Ni/Al layered double hydroxide [Ni/Al-LDH] intercalated by [NH $_3$ ], [SO $_4$ <sup>2-</sup>] and [CO $_3$ <sup>2-</sup>] as the main product, and accompanied by phases impurities.

From XRD patterns (Fig. 4a), the largest diffraction peaks were obtained at 2theta (20) Bragg angles of 10.745°, 22.101°, 34.922° and 61.067°, which are assigned to the crystalline planes, according to the Miller indices (hkl): (003), (006), (012), (110) respectively, are also of interest at 46.43° (018) and 72.676° (119). These diffraction peaks are indexed on a hexagonal system with rhombohedral symmetry, special group R-3m (polytype of three layers). The presence of 0kl peaks anticipates the presence of stacked layers (JCPDS file 15-0087). <sup>22,27,28,34,39,55</sup>

The XRD pattern also showed phases impurities. By comparison of the characteristic reflection pattern in Fig.4a to a reference library of samples, the low intensity peaks can be attributed to the bayerite polymorphs Al(OH)<sub>3</sub> and aluminum hydroxide or gibbsite [γ-Al(OH)<sub>3</sub>], (JCPDS 33-0018, JCPDS 20-0011, JCPDS 24-0006). 15,40,56 Also nickel hydroxide [Ni(OH)2] indexed to the hexagonal  $[\beta-Ni(OH)_2]$ , the  $[Ni(OH)_2 0.75H_2O]$ , nickel oxy-hydroxides corresponding to [ $\beta$ -NiOOH] and [ $\gamma$ -NiOOH] phases can be identified (JCPDS 14-0117, JCPDS 38-0715, JCPDS 06-0141, JCPDS 06-0075)<sup>57,58,59-61</sup> The presences of nickel aluminate were also identified: [NiAl<sub>2</sub>O<sub>4</sub>], [NiAl<sub>26</sub>O<sub>40</sub>], [NiAl<sub>32</sub>O<sub>49</sub>] and [Ni<sub>2</sub>Al<sub>18</sub>O<sub>29</sub>] (JCPDS 10-0339, JCPDS 20-0776, JCPDS 20-0777, JCPDS 22-0451).62,63 These phases may be a consequence of the decrease in pH during the process from 8.53 (+/-0.07) to 8.35 (+/-0.08).

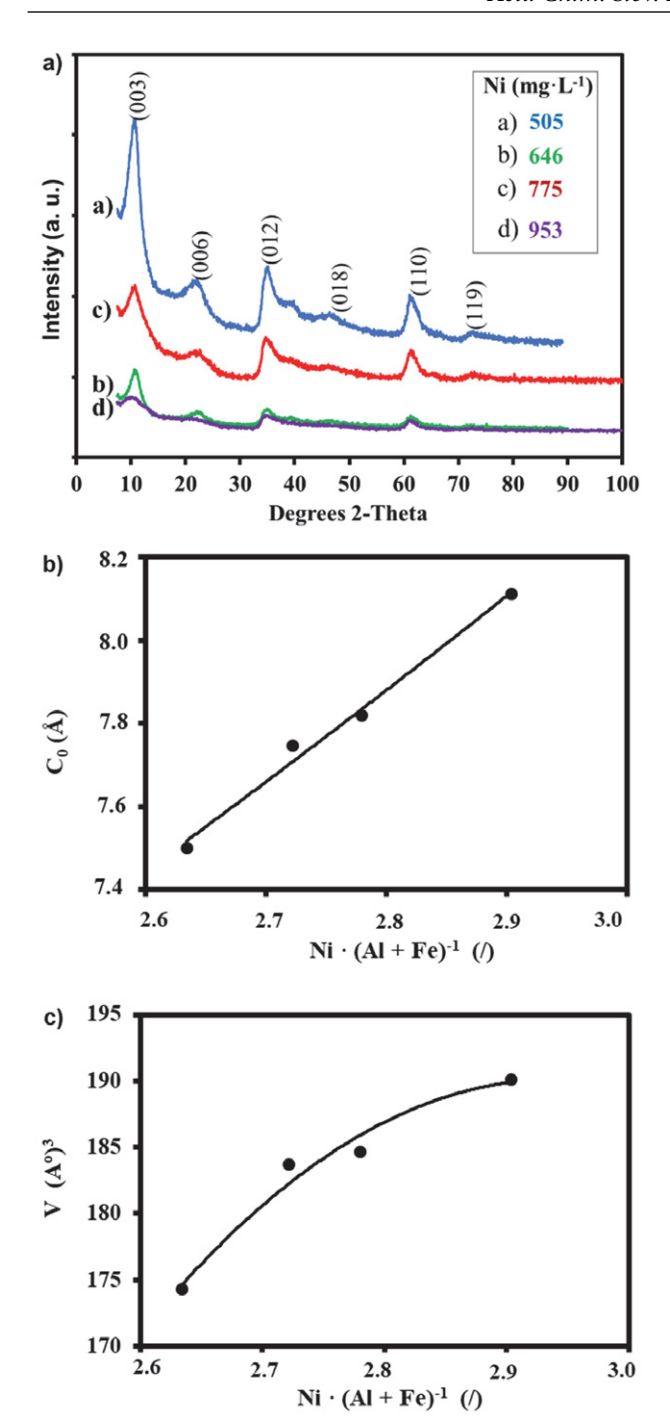


**Figure 4.** XRD of Ni/Al-LDH, Cu Kα1,  $\lambda$ =1.540598 Å, at 9.8 mA/cm², 30 min, 60 °C and pH 8.6. a) Diffraction intensity for various Bragg reflection angles. b) Interaction of the basal axis  $c_0$  with the molar ratio M(II)/M(III). c) Crystallite volume interaction V (Å)³ with M(II)/M(III).

Fourier transform infrared spectroscopy (FTIR) spectra of the samples are illustrated in Fig.5. The broad bands that can be seen in the region from 3423 to 3465 cm<sup>-1</sup> are assigned to the stretching vibrations hydroxyl group (vOH) in the Ni/Al -LDH, Ni(OH)<sub>2</sub>, Al(OH)<sub>3</sub> and

the water molecules adsorbed in the interlayer. 25,26,27,36,55 The peaks observed between 2077.9 and 2084.7 cm<sup>-1</sup> are associated with stretching vibration of the N-H bond.55 The characteristic bands between 1629 and 1641 cm<sup>-1</sup> are attributed the deformation of (HOH) angle of water molecule (δH-O-H) which confirms the presence of water in the Ni/Al-LDH interlayer. 17,21,25,26,36 The spectra also shows intense bands located from 1364 to 1368 cm<sup>-1</sup> and represent symmetric stretching vibrations carbon-oxygen bond (C-O) of carbonate ions  $n_3(CO_3^{2-})$ .  $^{20,21,55,60}$  The adsorption peaks from 1108 to 1115 cm<sup>-1</sup> corresponded to S-O stretching vibrations of the sulfate anion n<sub>3</sub>(-SO<sub>4</sub><sup>2-</sup>). <sup>20,24</sup> The characteristic band at 1041 cm<sup>-1</sup> represents the vibration v(Al-OH). Furthermore, in the region between 615 and 617 cm<sup>-1</sup> the bands can be assigned to the stretching vibration of metal (M) - oxygen (Ni-O; Al-O; Ni-O-Al), related to the oxides and aluminates determined by DXR.<sup>25,36</sup> The peaks between 409.8 and 410.8 cm<sup>-1</sup> are assigned to nickel oxides and nickel hydroxides [Ni-O; Ni-O-H<sup>-</sup>]; and the bands between 566 – 567 cm<sup>-1</sup> are attributed to stretching vibrations [Ni<sup>3+</sup>-O] in [γ-NiOOH]. <sup>14,25,60</sup>

The elemental analysis of the precipitates is given in Table 6. The precipitate had a nickel concentration between 33.40 and 40.68%, aluminum from 6.43 to 7.0% and charge density (x) from 0.256 to 0.36. When the initial concentration of nickel increased, there was a tendency to increase Ni in the precipitate. The table also shows that sulfate anion was predominant.

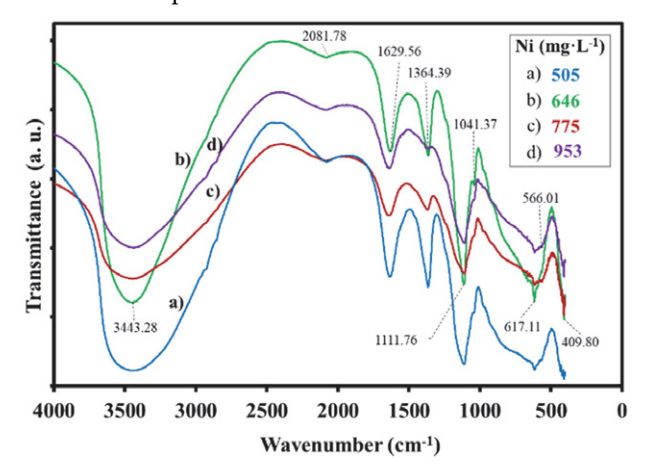


**Figure 5.** FTIR spectral of Ni/Al-LDH from different nickel concentration, a) 505 mg  $L^{-1}$ , b) 646 mg  $L^{-1}$ , c) 775 mg  $L^{-1}$ , d) 953 mg  $L^{-1}$ 

From the DXR analysis, the spacing  $(d_{hkl})$  of the LDHs, the crystal lattice parameters (a, c) and the crystallite size  $(D_{hkl})$  were determined (Table 7). Parameters "a" and "c" were calculated using the relationship between the spacing  $(d_{hkl})$  in the planes (hkl): (003), (012), (110) and the lattice parameters (a, b, c) for the hexagonal crystal system (b=c). The data was adjusted using the Statgraphic 5.1 software in the nonlinear regression option.

Table 6. Characterization of Ni/Al-LDH and estimated chemical formulas

[Ni <sup>2+</sup> ]	Concentration (%w/w)			Chemical formulas	Ni/(Al+Fe) (molar)	
	Ni	Al	S	Fe		
447	33.40	8.64	7.10	0.13	[Ni <sub>0.640</sub> Al <sub>0.360</sub> (OH) <sub>2</sub> ] (SO <sub>4</sub> ) <sub>0.156</sub> (CO <sub>3</sub> ) <sub>0.024</sub> xH <sub>2</sub> O	1.76
505	37.39	6.30	5.62	0.03	$[Ni_{0.732}Al_{0.268}(OH)_2] (SO_4)_{0.113} (CO_3)_{0.021} xH_2O$	2.72
646	38.47	6.67	5.72	0.09	$[Ni_{0.726}Al_{0.274}(OH)_2] (SO_4)_{0.123} (CO_3)_{0.014} xH_2O$	2.63
775	39.21	6.41	5.12	0.05	$[Ni_{0.738}Al_{0.262}(OH)_2] (SO_4)_{0.107} (CO_3)_{0.024} xH_2O$	2.80
953	40.68	6.43	4.37	0.02	[Ni <sub>0.744</sub> Al <sub>0.256</sub> (OH) <sub>2</sub> ] (SO <sub>4</sub> ) <sub>0.115</sub> (CO <sub>3</sub> ) <sub>0.013</sub> xH <sub>2</sub> O	2.90
1356*	39.20	7.00	3.75	0.05	[Ni <sub>0,720</sub> Al <sub>0,280</sub> (OH) <sub>2</sub> ] (SO <sub>4</sub> ) <sub>0,068</sub> (CO <sub>3</sub> ) <sub>0,071</sub> xH <sub>2</sub> O	2.57

\*Sample analyzed after electrocoagulation for 40 min

Table 7. Lattice parameters and size of Ni/Al-LDH crystallites

Sample Ni (g mL <sup>-1</sup> )		Spacing (Å)			rameters Å)	$V$ $(\mathring{A})^3$	Crystallite size (nm)	
	$d_{003}$	$d_{012}$	$d_{110}$	$\mathbf{a} = \mathbf{b}$	D		D	$D_{003}$
505	8.227	2.567	1.516	3.02	23.237	184	5.40	8.45
646	8.305	2.560	1.513	3.00	24.336	174	5.69	8.92
775	8.266	2.546	1.511	3.02	23.460	185	6.35	9.90
953	8.632	2.585	1.507	3.00	22.495	190	6.71	10.5

The distance between  $(d_{003~planes})$  of the LDH, also called d spacing, basal distance or thickness of the interlayer gallery was calculated using Bragg's Law. The obtained values were similar to those of the compounds synthesized by coprecipitation reported in the literature: [Ni/Al-SO<sub>4</sub><sup>2-</sup>]  $(8.01 \le d_{003} \le 8.59 \text{ Å})$  and [Ni/Al-NO<sub>3</sub><sup>-</sup>]  $(7.82 \le d_{003} \le 8.76 \text{ Å})$ . The variation in the basal distance is due to the variation in the amount (intercalation degree) and type of anions (atom size and valence) in the LDH interlayer.<sup>24,26,64</sup>

The average values of the lattice parameters (+/-standard deviation) were: a=b=3.01 Å (+/-0.013) and "c" equal to 23.4 Å (+/-0.76), with a fit quality greater than 99.7%, confirming that it is a hexagonal crystalline system. The parameter "a" is equivalent to the average distance between the center of adjacent cations in the lattice; and "c" is the basal axis, which is related to the distance between neighboring atoms and the interlayer distance. These parameters are comparable to the parameters reported for the compounds obtained by coprecipitation: [Ni/Al-SO<sub>4</sub><sup>2-</sup>]-LDH values of "a" 3.03 Å and "c" 24.05 Å; and for [Ni/Al-CO<sub>3</sub><sup>2-</sup>]-LDH in the following ranges:  $3.02 \le a \le 3.08$  Å and  $22.2 \le c \le 24.05$  Å. 21,24,28

The basal axis cell parameter for n-layers is c=n  $c_0$ . For the polytype 3R with rhombohedral symmetry n=3, and with the lowest reflection  $(0\ 0\ n)\ c_0$  (Å) was calculated. An increase in the basal axis as the molar ratio  $[Ni^{2+}/(Al^{3+}+Fe^{3+})]$  increases was observed with a coefficient of determination  $(R^2)$  equal to 97.42%. This is because the nickel has a larger ionic radius than iron and aluminum  $(0.69\ Å)$  > 0.55 Å > 0.535 Å), (Figure 4 b).  $^{21,26}$ 

The unit cell volume (V=0.866  $a^2$  c) was 183 Å<sup>3</sup> (+/-6.58), similar to other [CO<sub>3</sub><sup>2-</sup>]-LDH obtained by co-pre-

cipitation such as [Zn/Al] 189 ų, [Ni/Al] 187.6 ų y [Mg/Al] 180 ų and by the sol-gel method [Ni/Al] 148-163 ų, the lower the molar ratio [Ni²+/ (Al³+ + Fe³+)] the smaller the volume, (Figure 4 c). $^{21,28}$ 

The crystallite size ( $D_{hkl}$ ) was calculated using the Scherrer equation and the mean size (D) by the Williason-Hall "SSP" method. Both sizes reached lower values than other Ni/Al-LDHs synthetized by coprecipitation, but those were similar to the LDHs obtained by the sol-gel technique [Ni/Al-CO<sub>3</sub><sup>2-</sup>] (2.69  $\leq D_{003} \leq 8.11$  nm). Crystallinity increased with increasing temperature, current density and constant alkaline pH.  $^{21,34,65}$ 

In that order of ideas, the average size of the crystal-lites (D) presented an inversely proportional relationship with the reaction rate constant ( $k_{av}$ ) of the Avrami's model, fallowing a linear function ( $R^2$  95.92%). Regarding the fractional reaction order ( $n_{av}$ ), it was related to the preferential orientation of the crystallites, according to the peak intensity in the  $I_{003}/I_{012}$  ratio ( $1.43 \le I_{003}/I_{012} \le 1.82$ ) with an inverse relationship and linear trend ( $R^2$  98.0%). Liu (2015) used the ratio  $I_{003}/I_{012}$  in the interval  $0.2 \le I_{003}/I_{012} \le 2.7$  to evaluate the orientation of Ni/Al-CO<sub>3</sub>-LDH. He referred that a higher  $I_{003}/I_{012}$  value indicates that the LDH has a c-axis preferred orientation, while a lower value demonstrates preferentially ab-oriented. Based on this criterion, it was supposed that when the fractional reaction order (nav) increases the crystallites have a greater tendency to ab-orientation.  $^{43}$ 

#### 3. 4 Nickel Removal Mechanism Analysis

Taking into account the results of the kinetic and equilibrium analysis, the characterization of the product,

as well as the information consulted in the literature, it is considered that the following reactions control the nickel removing by electrocoagulation of Ni(II)-NH $_3$ -CO $_2$ -SO $_2$ -H $_2$ O system, (Fig. 6).  $^{6,7,10,11,15,66}$ 

- a) Precipitation of nickel hydroxide.
- b) Co-precipitation of Ni in spinels [Ni<sub>x</sub>Al<sub>v</sub>O<sub>z</sub>].
- c) Precipitation of layered double hydroxides.
- d) Cathodic electro-reduction to form metallic nickel

Where, the anionic ligands  $[CO_3^{2-}]$ ,  $[S_xO_y^{z-}]$ ,  $[NO_3^{2-}]$  on the coordination surface, depending on the dissolved Ni concentration, activate a synergism on the process that benefits the removal.

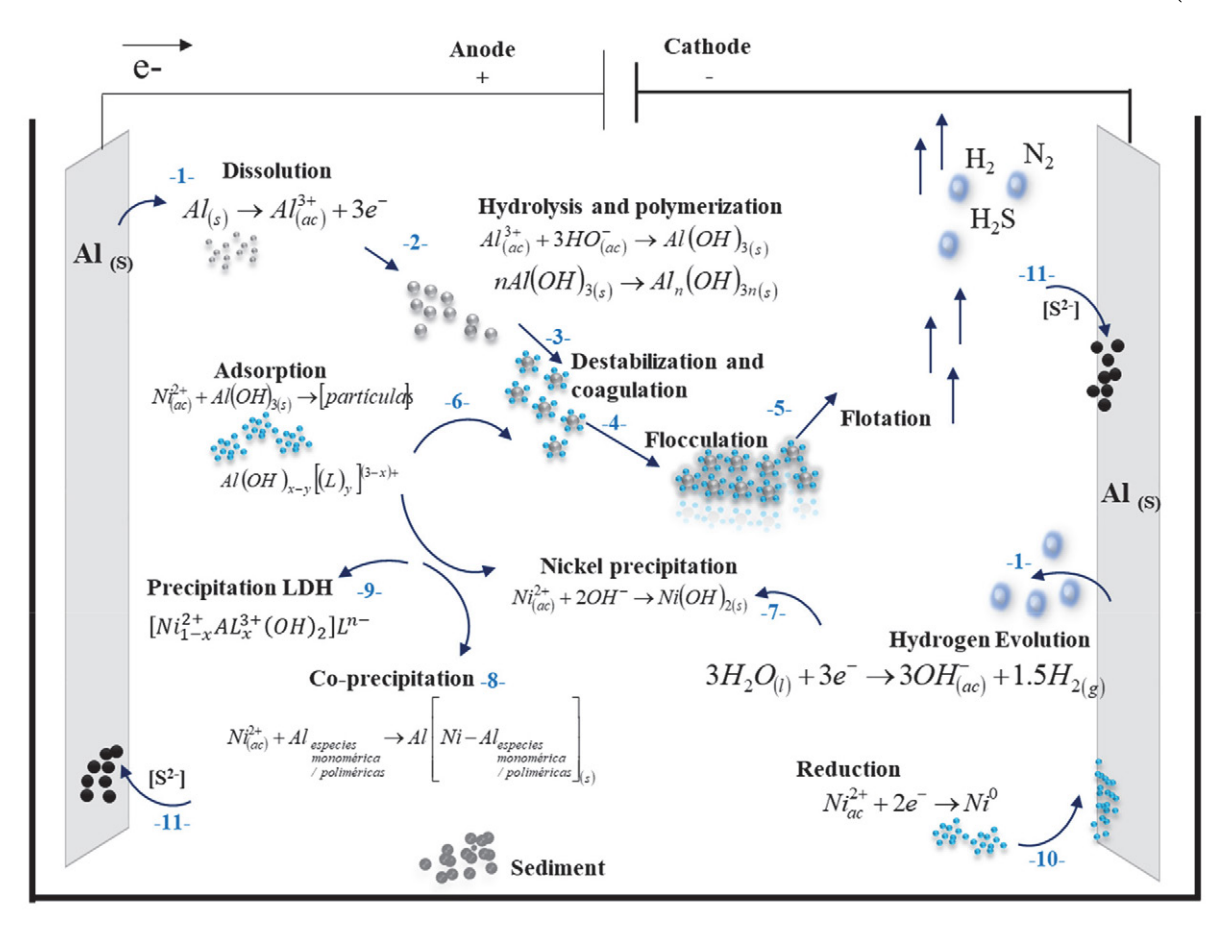
$$3H_2O_{(l)} + 3e^- \rightarrow 1.5H_{2(q)} + 3OH^-$$
 (47)

$$Al_{(ac)}^{3+} + 30H^{-} \rightarrow Al(0H)_{3(s)}$$
 (48)

$$nAl(OH)_{3(s)} \to Al_n(OH)_{3n(s)} \tag{49}$$

Nickel compounds and other contaminants, either colloids, suspended or dissolved material begin to destabilize due to:6,7,11,13

1) Compression of the diffuse double layer around the charged species because of the physical-chemical interactions with the generated ionic species, by the electrochemical dissolution of the sacrificial electrode (anode).



 $\textbf{Figure 6.} \ Schematic \ representation \ of \ the \ nickel \ removal \ mechanism \ by \ electrocoagulation \ of \ the \ Ni(II)-NH_3-CO_2-SO_2-H_2O \ system.$ 

Due to the simultaneous electrolytic reactions that occur on the surface of the electrodes (step 1 Fig. 6), the electro-coagulant aluminum cation [Al $^{3+}$ ] and the hydroxide anion [OH $^{-}$ ] are produced, Eq. (46) and (47). These diffuse in the solution and spontaneously the hydrolysis of aluminum occurs to form several monomeric and polymeric species, oligomeric complexes and aluminum hydroxide, Eq. (48) and (49), Step 2. $^{67}$ 

$$Al_{(s)} \to Al^{3+} + 3e^-$$
 (46)

These affect the potential difference between the surface of the particles and the solution, thus decreasing the interparticle repulsive forces.

2) Charge neutralization of the ionic species present in the solution due to the ions of opposite charge generated at the anode and the processes of adsorption, precipitation and co-precipitation; thus, the interparticle repulsive electrostatic forces decrease, instead the Van der Walls attraction forces predominate and as a result, coagulation occurs. While monomeric aluminum species neutralize the charge of contaminants by adsorbing on their surface and binding to their ionized groups, polymeric species can bind several contaminant particles (or molecules) at once, Step 3.

- 3) Following destabilization, flocs are formed as a result of aggregation of the destabilized particles, leading to sludge formation (flocculation), Step 4.
- 4) The hydrogen released in the cathodic reaction (2), enables the electro-flotation of the flocculated particles, which is also favored by the removal of sulfur in the form of hydrogen sulfide (H<sub>2</sub>S), Step 5.

In parallel, mechanisms occur that favor the removal of nickel, as explained below:

Adsorption of  $[Ni^{2+}]$  in the active centers of the surface of the aluminum species and fundamentally, on  $[Al(OH)_3]$  in interaction with other ions present in solution provided by the compounds  $CO_2$  -  $SO_2$  -  $NH_3$ . This process happens by two mechanisms: electrostatic attraction and coordination surface, Eq. (50), Step 6.

$$Ni^{2+} + Al(OH)_{3(s)} \rightarrow [particle]$$
 (50)

Result of simultaneous reactions at the anode and cathode, hydroxide ion is released and nickel hydroxide precipitates, Eq. (51), Step 7.

$$Ni^{2+} + 2OH^{-} \rightarrow Ni(OH)_{2(s)}$$
 (51)

Through sequential co-precipitation,  $[Ni(OH)_2]$  is incorporated into the crystal structure of  $[Al(OH)_3]$  and forms spinel:  $NiAl_2O_4$ ],  $[NiAl_{26}O_{40}]$ ,  $[NiAl_{32}O_{49}]$ ,  $[Ni_2Al_{18}O_{29}]$ , Eq. (52) and (53), Step 8.

$$Ni^{2+} + Al \begin{array}{c} monomeric \\ polymeric \end{array} \rightarrow Al \begin{array}{c} Ni - Al \begin{array}{c} monomeric \\ polymeric \end{array} \Big|_{(s)}$$
 (52)

$$2Ni(OH)_{2(s)} + Al(OH)_3 \rightarrow 2NiAl_2O_{4(s)}$$
 (53)

Anions in solution are attracted by electrostatic forces to balance charges and adsorbed on the active centers of the coordination surface, where (L) represents anionic ligands such as  $[{\rm CO_3}^{2-}], [{\rm S_xO_y}^{z-}], [{\rm NO_3}^{2-}], [{\rm OH^-}], {\rm Eq. (54)}$  and (55). <sup>65,68</sup>

$$Al(OH)_x^{(3-x)+} + yL^- \leftrightarrow Al(OH)_{x-y}[L_y]^{(3-x)+} + yOH^-$$
 (54)

$$mAl^{3+} + (3n-m)OH^{-} + mL^{-} \leftrightarrow Al_{m}(L)_{m}[OH]_{3n-m}$$
 (55)

Subsequently, the adsorbed ions can be displaced by other competing ions in the solution (exchange adsorption), due to the interactions between the ions on the charged surface and in the diffuse layer around the surface, and the nickel removal by formation of Ni-Al/LDH is promoted. LDH of high purity at alkaline pH and maximum temperature of 80 °C has been prepared by co-precipitation, Eqs. (56) - (57), Step 9. <sup>24,26,31,69,70</sup>

$$\left(1 - \frac{3}{2}x\right)Ni(OH)_2 + xAl(OH)_3 + 
+ \left(\frac{x}{2}\right)Ni(L^{n-})_{2/n} \leftrightarrow [Ni_{1-x}^{2+}Al_x^{3+}(OH)_2](L^{n-})_{x/n}$$
(56)

$$(1-x)Ni(OH)_2 + xAl(OH)_4^- + \left(\frac{x}{2}\right)(L^{n-})_{2/n}$$

$$\leftrightarrow \left[Ni_{1-x}^{2+}Al_x^{3+}(OH)_2\right]^{x+}(L^{n-})_{x/n} + 2xOH^-$$
(57)

The hydrogen evolution reaction (HER) (2) occurs at the cathode to a standard potential of -0.826 V with the release of gaseous  $H_2$ ; and the nickel reduction on the cathode surface to a more positive standard reduction potential of -0.25 V, Eq. (58), Step 10.

$$Ni^{2+} + 2e^- \to Ni_{(s)}$$
 (58)

The precipitation of [Ni(OH)<sub>2</sub>], [Ni/Al-LDH] and the co-precipitation of spinels Ni-Al cause a synergistic effect in the process, achieving high efficiency of nickel removing. A greater effect is reached as the initial nickel concentration in dissolution increases, which is reflected by the kinetic model TCV Eq. (45).

The possibility of an electrocatalytic effect of  $Ni^{2+}/Al^{3+}$ -LDH and the pair  $Ni(OH)_2/[\beta-Ni^{3+}OOH]$  on the anodic reaction of water electrolysis with oxygen evolution (OER) is also considered. The OER presupposes the absorption in the anode deposits of the hydroxide radicals generated by the hydrogen evolution (HER) in the cathode (0.404 V), Eq. (59).<sup>71</sup> The OER can promote the aluminum oxidation and the formation of LDH, Eq. (60) and (61).

$$30H^{-} \to \frac{3}{4}O_2 + \frac{3}{2}H_2O + 3e^{-} \tag{59}$$

$$2Al_{(s)} + \frac{3}{2}O_2 \to Al_2O_{3(s)} \tag{60}$$

$$Al_2O_3 + 3H_2O + 2OH^- \rightarrow 2Al(OH)_4^-$$
 (61)

The intercalation of molecules ( $H_2O$ ,  $NH_3$ ) and anions [ $S_xO_y^{z-}$ ], [ $CO_3^{2-}$ ] in the LDH interlayer let to more electrons could being transferred to the surface of the active sites of LDH [ $Ni_{1-x}Al_xOOH$ ], stabilizing their high-valence states and increases the activity for the OER from the reversible redox pair  $Ni^{2+}/Ni^{3+}$ . Zhou et al. (2018) showed that intercalated anions with strong reducing ability modify the electronic structure of surface metal sites and significantly improve the performance of the corresponding LDH for the OER with a linear relationship<sup>64</sup>, in the case of ions [ $S_xO_v^{z-}$ ] it increases from [ $S_2O_8^{2-}$ ] to [ $SO_3^{2-}$ ].

Regarding NiOOH, it is a catalyst for OER under alkaline conditions and acts as an active center in the pair  $[Ni(OH)_2]/[\beta-NiOOH]$  for the adsorption of  $[OH^-]$ . Nickel is capable of acquiring valences (+2, +3, +3.6) making it susceptible to various electronic transitions and phase transformations, Eq. (62). The  $Ni(OH)_2$  has a large specific surface which favors contact between the active material

and the electrolytic dissolution. 59,72,73,74

Reactions of sulfide formation (NiS,  $Al_2S_3$ ), the release of irritating gases ( $H_2S$ ) and the formation of deposits on the surface of the electrodes are considered. These deposits exert resistance to the passage of electrical current, reduce charge transfer, affect the efficiency of the process and the stability of the operation, Step 11.

# 3. 5 Result of the Operating Cost Estimate

The operating cost was estimated for electrode and electrical energy consumption for initial nickel concentration in the range  $0.474 \le \text{Ni} \le 0.953 \text{ g L}^{-1}$ ,  $9.8 \text{ mA cm}^{-2}$ ,  $60 \, ^{\circ}\text{C}$ , pH 8.6 and 98% nickel removal, for a remainder between 6 and 19 mg L<sup>-1</sup> (Table 8).

**Table 8.** Estimated operating costs for nickel removal by electrocoagulation Base: 98% removing, 9.8 mA cm<sup>-2</sup>, 60 °C, pH 8.6

Ni (mg L <sup>-1</sup> )	379	447	505	646	775	953
Cost (\$ t <sup>-1</sup> Ni)	320	382	509	521	537	534
SEC (kW h kg <sup>-1</sup> Al)	5.26	6.33	6.75	5.11	3.45	2.76

The operating cost amounted to between 320 and 537 \$ t^{-1}\$ of nickel removed, regarding the specific energy consumption (SEC), it was between 2.76 and 6.75 kW h kg<sup>-1</sup> of aluminum. The increase in nickel concentration in the initial liquor augments the electrocoagulation time necessary to achieve high removal efficiency and therefore also increases energy and electrode consumption. The higher the concentration of ionic species in the liquor, the conductivity is favored and SEC decreases.

According to the analyzed aspects of the removal mechanism, it is possible to reduce costs by designing a reactor with favorable geometric and hydrodynamic conditions to achieve adequate mass transfer between the phases. It also suggests recycling a suspension of the product obtained at the non-saturation conditions of the adsorption sites, according to the isotherm model to be followed.

#### 4. Conclusions

The nickel removing by electrocoagulation from the liquor effluent of the nickel production plant in Punta-Gorda Cuba, was studied in Ni(II)-NH<sub>3</sub>-CO<sub>2</sub>-SO<sub>2</sub>-H<sub>2</sub>O system. The reaction kinetics, the adsorption isotherm, the mechanism and the preliminary cost of operation at different concentrations of dissolved nickel in the initial liquor were evaluated. In the interval defined for the operating

variables, a removing efficiency between 97.7 and 99.7% was obtained. A kinetic model of conversion time was proposed, which suggests that the process is determined by the combined effect of the resistances of the mechanisms: external diffusion, nucleation, and as controlling step the chemical reaction and a possible autocatalytic contribution. The removal was characterized by monolayer chemisorption at a finite number of specific adsorption sites, following the Langmuir isotherm. The precipitate had between 33.4 and 40.7% nickel and from 6.3 to 7.0% aluminum, with a typical structure of Ni/Al-LDH and phases impurities Al(OH)3, Ni(OH)2/NiOOH and nickel-aluminum spinels. The operating costs were between 320 and 537 \$ t<sup>-1</sup> of removed nickel, considering the energy and electrode consumption. The research represents the opportunity to diversify production, in-situ synthesize Ni/Al-LDH, improve its properties and evaluate its applications for the projection of an industrial process.

#### Acknowledgment

Thanks to Nélida Powery Ebanks, NICAROTEC Co.; and colleagues of the Chemical Analysis Laboratory, CED-INIQ-Nicaro Cuba, for their collaboration.

#### Conflict of Interest

The authors declare no conflict of interest

#### 5. References

- A. R. Vargas; M. E. T. Nieves; Y. G. Díaz. Acta Chimica Slovenica, 2020, 67, 1239–1249. DOI:10.17344/acsi.2020.6147
- A. R. Vargas, M. E. M. Haynes, A. R. Riveron. *Rev. Metal. (Madrid, Spain).* 2019, 55, DOI:10.3989/revmetalm.149
- L. C. Lamorú, A. O. C. Navarro, Y. A. Arias. *Minería y Geología*. 2018, 34, 422–439.
- A. R. Vargas, A. R. Riverón, M. P. Medina, E. O. Armaignac. Tecnol. Quim. 2020. 40, 363–382.
- 5. L. M. Irions, A. R. Vargas, et al. Tecnol. Quim. 2020, 40, 19-36.
- A. S. Naje, S. Chelliapan, Z Zakaria, M A. Ajeel, P A Alaba. Rev. Chem. Eng. 2016, 33, 263–292.

DOI:10.1515/revce-2016-0019

- 7. J. N. Hakizimana, B. Gourich, M. Chafi, et al. *Desalination*. **2017**, *404*, 1–21. **DOI**:10.1016/j.desal.2016.10.011
- 8. S. García-Segura, M. M. S. G. Eiband, J. Vieira de Melo, C. A. M. Huitle. *J. Electroanal. Chem.* **2017**, 801, 267–299. **DOI:**10.1016/j.jelechem.2017.07.047
- 9. Z. Al-Qodah, M. Al-Shannag, K. Bani-Melhem, et al. *Environ. Chem. Lett.* **2018**, *16*, 695–714.

**DOI:**10.1007/s10311-018-0711-1

- Z. Al-Qodah, M. Al-Shannag. Sep. Sci. Technol. 2017, 52, 2649–2676. DOI:10.1080/01496395.2017.1373677
- S. M. Didar; U. I. Islam. Sustain. Water Resour. Manag. 2019, 5, 359–380. DOI:10.1007/s40899-017-0152-1

- 12. K. Dermentzis, K. Karakosta, R. Kosheleva, N. Kokkinos. *J. Eng. Sci. Tech. Rev.*, **2020**, *13*. **DOI**:10.25103/jestr.136.04
- 13. D. Ghernaout, A. Alghamdi, B. Ghernaout. *J. Environ. Sci. Allied. Res.* **2019**, 51–67.
- 14. T. S. Pertile, E. J. Birriel. *Korean J. Chem. Eng.* **2017**. *34*, 2631–2640. **DOI:**10.1007/s11814-017-0178-y
- 15. X. Chen, P. Ren, Tao Li, et al. *Chem. Eng. Journal.* **2018**, *31*, 358–367. **DOI**:10.1016/j.cej.2018.05.099
- H. Zhao, B. Zhao, W. Yang, T. Li. Environ. Sci. Technol. 2010, 44, 9112–9116. DOI:10.1021/es102540t
- 17. M. M. Mendoza, D. D. Victoria, N. M. Cabrales. *MethodsX*. **2018**, *5*, 915–923. **DOI**:10.1016/j.mex.2018.07.019
- L. Jiang, G. Huang, L. Shao, J. Huang, S. Peng, X. Yang. Colloids Surf. 2021, 608, 125589.
  - DOI:10.1016/j.colsurfa.2020.125589
- 19. Ou, J. Yan, T. Xu, Z. Jiang, H. Tan, S. He, B. Hu, G. Yu. *J. Mol. Liq.* **2021**, *335*, 116246. **DOI**:10.1016/j.molliq.2021.116246
- Y. Zhao, F. Xiao, Q. Jiao. J. Nanotechnol. 2011.
   DOI:10.1155/2011/646409
- M. Jitianu, D. C. Gunness, D. E. Aboagye, M. Zaharescu, A. Jitianu. *Mater. Res. Bull.* 2013, 48, 1864–1873.
   DOI:10.1016/j.materresbull.2013.01.030
- T. D. Nguyen, Q. T. P. Bui, H. Q. H. Phan. J. Mater. Sci. Surf. Eng. 2016, 4, 488–491.
- L. Li, K. S. Hui, K. N. Hui, et al. J. Alloys Compd. 2017.
   DOI:10.1016/j.jallcom.2017.06.062
- 24. F. Z. Mahjoubi, A. Khalidi, M. Abdennouri, N. Barka. *Desalin. Water Treat.* **2015**, 1–13.
  - DOI:10.1080/19443994.2015.1124055
- 25. F. Z. Mahjoubi, A. Elhalil, R. Elmoubarki, et al. *JASI*. **2017a**, *2*(*1-3*), 1–11.
- F. Z. Mahjoubi, A. Khalidi, O. Cherkaoui, et. al. *J. Water Reuse Desalin.* 2017b. DOI:10.2166/wrd.2016.041
- S. Jaerger, S. F. Zawadzki, A. Leuteritz, F. Wypych. *J. Braz. Chem. Soc*, 2017, 28, 2391–2401.
  - **DOI:**10.21577/0103-5053.20170093 8. W. M. A. El Rouby, S. L. El-Dek, M. E. Gol
- W. M. A. El Rouby, S. I. El-Dek, M. E. Goher, S. G. Noaemy. *Environ. Sci. Pollut.* Res. 2018.
   DOI:10.1007/s11356-018-3257-7
- O. Rahmanian, M. H. Maleki, M. Dinari. J. Phys. Chem. Solids. 2017, 110, 195–201. DOI:10.1016/j.jpcs.2017.06.018
- N. Taoufik, W. Boumya, A. Elhalil, et al. *Int. J. Environ. Anal. Chem.* 2020. DOI:10.1080/03067319.2020.1863387
- 31. M. Mousazadeh, S. M. Alizadeh, Z. Frontistis, et al. *Water*. **2021**, *13*, 656. **DOI**:10.3390/w13050656
- Z. Tang, Z. Qiu, S. Lu, X. Shi. Nanotechnol. Rev. 2020. 9, 800
   BOI:10.1515/ntrev-2020-0065
- 33. H. Lu, Q. Li, H. Xiao, et al. Am. J. Anal. Chem. **2014**. *5*, 547–558. **DOI:**10.4236/ajac.2014.59062
- L. Yang, Z. Liu, S. Zhu, L. Feng, W. Xing. *Materials Today Physics*. 2021, *16*, 100292. DOI:10.1016/j.mtphys.2020.100292
- N. Ayawei, A. N. Ebelegi, D. J. Wankasi. J. Chem. 2017.
   DOI:10.1155/2017/3039817
- M. Mamat, N. Roslan, K. H. K. Bulat, et al. Mater. Sci. Eng. 2018, 440. DOI:10.1088/1757-899X/440/1/012013
- 37. G. Li, X. Zhang, D. Qiu. Adv. Electron. Mater. 2019, 5,

- 1900215. **DOI:**10.1002/aelm.201900215
- X. Zhang, C. B. Cockreham, E. Yılmaz. *ChemRxiv*. 2020. DOI:10.26434/chemrxiv.11919804.v2
- J. Wang, Y. Song, Z. Li. Energy Fuels. 2010, 24, 6463–6467.
   DOI:10.1021/ef101150b
- W. Wang, N. Zhanga, Z. Shia. Chem. Eng. J. 2018, 338, 55–61.
   DOI:10.1016/j.cej.2018.01.024
- 41. Q. Xie, Z. Cai, P. Li, et al. *Nano Res.* **2018**, *11*, 4524–4534. **DOI**:10.1007/s12274-018-2033-9
- 42. M. Gabrovska, D. Nikolova, M. Shopska, et al. W. E. Lee et al. (eds.), Proceedings of the III Advanced Ceramics and Applications Conference. **2016**.
  - **DOI:**10.2991/978-94-6239-157-4\_15
- 43. Y. Liu, T. Yu, R. Cai. *RSC Adv.* **2015**, *5*, 29552. **DOI**:10.1039/C5RA01969A
- S. Iguchi, S. Kikkawa, K. Teramura, et al. *Phys. Chem. Chem. Phys.* 2016, *18*, 13811–13819. DOI:10.1039/C6CP01646D
- M. Gabrovska, R. E. Kardjieva, D. Crisan, et al. *Reac. Kinet. Mech. Cat.* 2012, *105*, 79–99.
   DOI:10.1007/s11144-011-0378-0
- 46. F. Touahra, M. Sehailia, W. Ketir, et al. *Appl. Petrochem. Res.* **2016**, *6*, 1–13. **DOI:**10.1007/s13203-015-0109-y
- 47. E. C. Lima, A. R. Cestari, M. A. Adebayo. *Desalin. Water Treat.* 2015, 56, 19566–19571.
  DOI:10.1080/19443994.2015.1095129
- 48. H. N. Tran, S. J. Youb, A. H. Bandegharaei, H. P. Chao. *Water Res.* **2017**, *120*, 88–116. **DOI:**10.1016/j.watres.2017.04.014
- 49. A. I. Adeogun, R. B. Balakrishnan. *Appl Water Sci.* **2015**, *7*, 1711–1723. **DOI**:10.1007/s13201-015-0337-4
- A. A. Inyinbor, F. A. Adekola, G. A. Olatunji. Water Resour. Ind. 2016, 15, 4–27. DOI:10.1016/j.wri.2016.06.001
- N. A. Oladoja. Desalin. Water Treat. 2015, 57, 15813–15825.
   DOI:10.1080/19443994.2015.1076355
- 52. A. R. Vargas. Tecnol. Quim. 2021, 42, 114-130.
- I. Avramov, J. Sestak. Generalized kinetics of overall phase transition explicit to crystallization. *J. Therm. Anal. Calorim.* 2014, 118, 1715–1720. DOI:10.1007/s10973-014-4144-1
- 54. L. Shi-Yong, Z Jia-yun, Z. Tu-ping. Computer prediction system on solid / solid reaction kinetic. Trans. Nonferrous Met. Soc. China. **2001**, *11*(*3*), 466–470. **DOI**: 1003-6326(2001) 03-0466-05.
- X. Xue, S. Zhang, H. Zhang. Am. J. Anal. Chem. 2015, 6, 334–341. DOI:10.4236/ajac.2015.64032
- N. F. M. Salleh, A. A Jalila, S. Triwahyonoc, et al. *Appl. Surf. Sci.* 2015, 349, 485–495. DOI:10.1016/j.apsusc.2015.05.048
- 57. P. Lu, F. Liu, D. Xue, et al. *Electrochim. Acta.* **2012**, *78*, 1–10. **DOI:**10.1016/j.electacta.2012.03.183
- D. S. Hall, David; D. J. Lockwood, C. Bock, B. R. MacDougall. *Proc. R. Soc. A.* 2015, 471. DOI:10.1098/rspa.2014.0792
- M. H. Syafiq, O. M. Rozali. Int. J. Electrochem. Sci. 2018, 8, 4747–4760.
- A. A. Lobinsky, V. P. Tolstoy, I. A. Kodinzev. *Nanosyst.: Phys.*, *Chem.*, *Math.* **2018**, 9, 669–675.
   **DOI:**10.17586/2220-8054-2018-9-5-669-675
- A. Khan, R. A. Senthil, J. Pan, Y. Sun. Chin. J. Chem. Eng. 2019. DOI:10.1016/j.cjche.2019.01.025

- 62. C. G. Anchieta, L. Tochetto, H. B. Madalosso. *Cerámica*. **2015**, *61*, 477–481. **DOI**:10.1590/0366-69132015613601925
- 63. C. Ragupathi, J. J. Vijaya, J. L. Kennedy. *J. Saudi Chem. Soc.* **2017**, *21*, 231–239. **DOI:**10.1016/j.jscs.2014.01.006
- D. Zhou, Z. Cai, Y. Bi. Nano Res. 2018.
   DOI:10.1007/s12274-017-1750-9
- 65. Y. T. Prabhu, K. V. Rao, V. S. Kumar, B. S. Kumari. *World J. Nano Sci. Eng.* **2014**, *4*, 21–28. **DOI:**10.4236/wjnse.2014.41004
- E. Nariyan, M. Sillanpää, C. Wolkersdorfer. Sep. Purif. Technol. 2017, 177, 363–373. DOI:10.1016/j.seppur.2016.12.042
- B. Lekhlif, L. Oudrhiri, F. Zidane, et al. J. Mater. Environ. Sci. 2014, 5, 111–120.
- M. A. Sandoval, J. L. Nava, O. Coreño, et al. Int. J. Electrochem.
   Sci. 2017, 12, 1318–1330. DOI:10.20964/2017.02.08

- J. J. Bravo-Suárez, E. A. Páez-Mozo, S. T. Oyama. Quim. Nova,
   2004, 27, 601–614. DOI:10.1590/S0100-40422004000400015
- 70. R. Bloom, N. Hondow, V. Dupont, M. V. Twigg, S. J. Milne. *Energy Rep.* **2018**, *4*. 733–743. **DOI:**10.1016/j.egyr.2018.10.008
- 71. Y. Cheng, S. P. Jiang. *Prog. Nat. Sci.: Mater. Int.* **2015**, *25*, 545–553. **DOI:**10.1016/j.pnsc.2015.11.008
- 72. D. E. Pissinis, L. E. Sereno, J. M. Marioli. *Open J. Phys. Chem.* **2012**, *2*, 23–33. **DOI:**10.4236/ojpc.2012.21004
- V. Kotok, V. Kovalenko, V. Malyshev. East. Eur. J. Enterp. Technol. 2017, 89, 5–12. DOI:10.15587/1729-4061.2017.109770
- 74. Y. H Chung, I. Jang, J. H. Jang. Sci. Rep. **2017**, *7*, 8236. **DOI:**10.1038/s41598-017-08296-0

## Povzetek

Raziskava poroča o odstranjevanju niklja z elektrokoagulacijo sistema Ni(II)-NH $_3$ -CO $_2$ -SO $_2$ -H $_2$ O v laboratorijskem merilu. Poskusi so bili izvedeni z Al/Al par elektrodami pri začetni koncentraciji niklja med 293 in 1356 mg L $^{-1}$  in pri obratovalnih parametrih pH 8,6, gostoti toka 9,8 mA cm $^{-2}$ , času elektrolize 30 min in temperaturi 60 °C. Dobljeni rezultati kažejo na učinkovitost odstranjevanja med 97,7 in 99,7 %. Kinetično modeliranje je predlagalo kombinirane učinke zunanje difuzije in nukleacije ter kemično reakcijo in možen avtokatalitični prispevek kot kontrolni korak. Postopek je sledil Langmuirjevi izotermi z največjo adsorpcijsko zmogljivostjo 7519 mg g $^{-1}$ . ICP-OES, XRD in FTIR karakterizacija oborin je pokazala tipične plastne Ni-Al dvojne hidroksidne strukture s 33,4 $^-$ 40,7 % niklja in 6,3 $^-$ 7,0 % aluminija, odvisno od začetne koncentracije niklja. Operativni stroški porabe energije in elektrod so bili 320 $^-$ 537 \$ t $^-$ 1 odstranjenega niklja.



Except when otherwise noted, articles in this journal are published under the terms and conditions of the Creative Commons Attribution 4.0 International License